Augmented Ensemble Calibration of Lumped-Parameter Building Models

Carlos Andrade-Cabrera[a], William J. N. Turner[b], Donal P. Finn[a]

[a] School of Mechanical and Materials Engineering, University College Dublin, Belfield, Dublin 4, Ireland
[b] School of Electrical and Electronic Engineering, University College Dublin, Belfield, Dublin 4, Ireland

Abstract

The dynamic integration of building retrofit investment tools and linear power systems optimisation tools requires the development of simplified linear building energy models which are representative of different Energy Conservation Measures (ECMs) options. Ensemble Calibration is a methodology which identifies linear building energy models as functions of ECMS for opaque building envelope components. The methodology uses Particle Swarm Optimisation (PSO), a heuristic optimisation algorithm, to minimise the calibration error between model predictions and suitable baseline data. The Ensemble Calibration methodology cannot model fast building thermal response characteristics, such as glazing parameters (e.g., thermal transmittance and solar transmittance) or air leakage parameters (e.g., infiltration rate), as functions of transparent envelope ECMs. The standard PSO algorithm widely explores the solution space while attracting all particles (i.e., candidate model solutions) to the best solution at each iteration. Fast building response parameters are significantly altered during the early iterations the PSO algorithm, thus having a negative impact of the overall calibration process. Therefore, the glazing and infiltration parameters are not correctly identified in an Ensemble Calibration framework and calibration accuracy of the building models suffers as a result. The current paper addresses this issue through the augmentation of existing Ensemble models using supplementary retrofit parameter functions for non-opaque ECMs. The paper also proposes a simplified infiltration model which emulates improvements in air tightness associated with the addition of ECMs while enabling other air tightness measures to be included as ECMs. The proposed methodology is applied to the Ensemble Calibration of an EnergyPlus archetype model representative of the detached housing stock in Ireland. The augmentation algorithm results in the accurate calibration of linear building energy models for different ECM configurations (i.e., ECM combination options), while providing considerable computational advantages. The proposed methodology enables the use of glazing and infiltration scenarios in an Ensemble Calibration framework, thus enhancing the representativeness of the methodology for the integrated analysis of ECM investment planning under future electrified space heating scenarios.

Keywords: Building retrofit; model calibration; ensemble calibration; building-to-grid; integrated analysis

Nomenclature

Variables and parameters

α	Calibration parameter (Ensemble Calibration) [-]
β	Calibration parameter (Ensemble Calibration) [-]
μ	Calibration parameter (Augmented Ensemble Calibration) [-]
ν	Calibration parameter (Augmented Ensemble Calibration) [-]
C	Lumped Capacitance $[J/kgK]$
Δx	Variation in layer thickness increment [mm]
F	Set of fixed parameters (calibration)
$J(\cdot)$	Calibration cost function
g	Solar transmittance (Window) [-]
l	Optimisation time-step (PSO)
M	Index for external insulation (Ensemble)
N	Index for internal insulation (Ensemble)
NH	Calibration horizon [time steps]
O	Index for ceiling insulation (Ensemble)
p	Set of calibration parameters
Q	Heating Load $[W]$
R	Lumped Resistance $[m^2K/W]$
T	Temperature [°C]
U	Thermal Transmittance (U-value) $[W/m^2K]$
V	Set of variable parameters (calibration)

Subscripts

0	Baseline model (Calibration parameters)
att	Attic
amb	Outdoor temperature
c	Ceiling node
$ceil$	Ceiling Insulation
$data$	Synthetic data
ext	External Insulation
gnd	Ground node
$heat$	Heat input

int	Internal Insulation
inf	Infiltration
k	Time-step index (Building model thermal evolution)
L	Time-step index (Particle Swarm Optimisation)
R	Room temperature
s	Solar gains
$wall$	External walls
win	Window
w	Wall node

Superscripts

$\star$	Optimal (calibrated) parameter

Acronyms

ACH	Air Changes per Hour
$BEMS$	Building Energy Model Simulation
$CV(RMSE)$	Coefficient of Variation of Root Mean Square Error
ECM	Energy Conservation Measure
EPS	Expanded Polystyrene
$IWEC$	International Weather for Energy Calculations
MAE	Mean Absolute Error

1. Introduction

1.1 Integrated building-to-grid analysis using Ensemble Calibration

Stabilizing global average temperature increase to below 2°C will likely avert the most dangerous effects of climate change impacts (IPCC 2014). This goal has been adopted by most of the developed countries under the United Nations Framework Convention on Climate Change (UNFCCC) (Alley et al. 2016). In a European context, European Energy Agency (EEA) projections show that significant progress has been made towards reaching the European carbon emission targets for 2020 (i.e., a reduction of 20% of residential emissions below pre-1990 levels by 2020 (EEA 2015). While encouraging, the EEA projections also show that current technologies will not be sufficient to achieve the desired long-term emission targets for 2050 (i.e., reduction by 80-95% below 1990 levels by 2050 (ECF 2010). Achieving the 2050 targets implies a reduction of 95% of residential emissions and the complete decarbonisation of the power sector (ECF 2011). One comprehensive mechanism which contributes towards the simultaneous achievement of these tasks consists of the integration of electrified space heating alongside other energy conservation measures (ECMs) for the existing building stock. Under this mechanism, the carbon emissions associated with the residential sector may be entirely abated due to the efficient usage of renewable power generation.

Building energy archetypes are increasingly used in the study of aggregated residential demand at the urban and national level (Reinhart and Davila 2016). These archetypes are often developed using Building Energy Model Simulation (BEMS) tools. Jermyn and Richman (2016) developed three archetypes representative of the Toronto residential building stock. The models were later used for the analysis of retrofit investment planning via automated optimisation. Cerezo et al. (2017) compared four archetype characterization methods using metered data from 365 residential dwellings from Kuwait City. The archetypes were developed in the EnergyPlus simulation environment. The study showed that probabilistic characterisation methods resulted in energy predictions that closely matched residential metered energy consumption data. Sokol et al. (2017) used a Bayesian approach for the calibration of EnergyPlus archetypes generated using GIS information and metered data from Cambridge, Massachusetts. Muringathuparambil et al. (2017) used DesignBuilder and EnergyPlus to define representative low cost building types in Cape Town.

BEMS are numerical solvers which iteratively try to identify operational parameters of the building energy model such as heating/cooling loads, airflow rates, etc. BEMS tools were originally conceived as tools to assist building energy performance design, and therefore model integration is not an intrinsic feature of the tools. On the other hand, power systems models are usually modelled as Mixed Integer Linear Programming (MILP) problems (Pudjianto, Aunedi, Djapic, and Strbac, 2014; Bakirtzis, Biskas, and Chatziathanasiou, 2012). BEMS and power systems models are therefore numerically incompatible. One potentially sub-optimal integration methodology consists of the pre-calculation of energy requirements or heating loads using BEMS archetypes. The pre-calculated residential energy requirements are then added to a multi-energy systems model. Wu et al. (2017) simulated energy demands from archetypes for the Swiss village of Zernez. The archetypes were developed using the EnergyPlus building simulation

environment. Ault et al. (2013) used building models representative of a Shetland housing state in order to calculate the aggregated heat demand forecast for the entire estate at 15 minute intervals. The models were developed using the ESP-r building simulation environment. The electrified heat demand forecast was then used as an input to a power system model which produces the optimal charging schedule for the estate.

The pre-calculation of electricity-demand time series can potentially incorporate ECM decision making by means of pre-calculating post-retrofit heating demand time series. The time series are then used in a power systems optimisation framework. One potential disadvantage of such an approach consists of the omission of building flexibility (i.e., storage in building fabric) and electricity grid flexibility (e.g., wind power availability). For example, an excess of available wind power can be dispatched to electricity storage devices (e.g., batteries or storage heaters), thus reducing wind curtailment and potentially reducing generation costs. A fully flexible solution requires the co-optimisation of the building energy models and power systems models. For the tractable co-optimisation of archetype building energy models and power systems models it is desirable that archetype building energy models are specified using a linear framework. Ensemble Calibration (Andrade-Cabrera et al. 2017) is a building model calibration technique which calibrates a number of lumped-parameter building models using pre and post-retrofit synthetic data. In this framework, every calibrated model corresponds to a different ECM configuration (i.e., a combination of ECM options). The advantage of Ensemble Calibration is that the final building energy models are linear matrix combinations of the pre-retrofit building model and linear model variations due to the building model variations post-retrofit. Therefore, using a linearisation heuristic, it is possible to determine the optimal retrofit configuration under electrified heating systems by co-optimising all retrofitted buildings and the grid model at the same time, instead of co-optimising every retrofitted building model with the grid model. The latter approach (i.e., a brute search approach) becomes computationally intractable when the number of retrofit configurations increases or when the power systems model is complex to solve.

1.2 Limitations of Ensemble Calibration

The previous contribution (Andrade-Cabrera et al. 2017) showed that the accuracy of the Ensemble Calibration algorithm is significantly reduced when model parameters representative of fast model dynamics (e.g., window retrofit) were selected as variable parameters and thus modelled through a retrofit function. The Ensemble Calibration framework relies on Particle Swarm Optimisation (PSO), a heuristic optimisation algorithm, to calibrate the models via the minimisation of an error cost function (i.e., mismatch between the synthetic data and the modelled temperature response). The algorithm is based on a randomized self-improvement of each candidate solution (i.e., a set of building model parameters) after each iteration. The automated manipulation of parameters representative of fast model dynamics (e.g., glazing parameters or air infiltration rate) results in a rapid reduction of the error cost function during the early iterations of the PSO algorithm, regardless of whether the identified parameters accurately represent all retrofitted models. These interactions have a negative effect on the accuracy of the Ensemble Calibration methodology.

Furthermore, Ensemble Calibration focused exclusively on the calibration of ECMs applied to the opaque components of the building fabric (i.e., walls, ceilings and roofs). In the Ensemble Calibration framework, the opaque fabric ECMs must be defined as monotonically increasing in evenly spaced increments (e.g., incremental steps of 10 mm in external insulation). This is not an issue with opaque fabric ECMs, as it is easy to obtain models with customized insulation thicknesses (e.g., 150 mm of external insulation in lieu of 100 mm) by means of calculating the retrofit function post Ensemble Calibration. However, it is likely that the window replacement scenarios to be considered might not appear in evenly spaced increments or decrements of the relevant physical magnitude (e.g., thermal transmittance). For example, consider the case where an existing double-glazing window with a thermal transmittance of 3.2 W/m^2K is to be replaced with either an energy efficient double-glazing uPVC window (1.6 W/m^2K) or a triple-glazing window (0.9 W/m^2K). The proposed window retrofit measures are not represented in evenly spaced increments and therefore, they are not suitable for direct implementation in an Ensemble Calibration framework.

For the Ensemble Calibration method to be complete, there is a requirement of formulating an extended methodology which enables the incorporation of unevenly spaced glazing and infiltration ECMs within the Ensemble Calibration framework.

1.3 Contributions

The current paper introduces a methodology to include glazing and infiltration information in previously calculated Ensemble models. It is demonstrated, from a numerical perspective, that the augmentation of Ensemble models enables the incorporation of glazing and infiltration information in Ensemble models using a model augmentation mechanism. In addition, an infiltration model is defined which considers the improvements of airtightness due to the implementation of single or multiple ECMs. These mechanisms are shown to be computationally efficient with respect to the equivalent Ensemble Calibration problem. The results of the application of the proposed methodology are demonstrated using a detached house archetype model. The paper shows the advantages of the proposed methodology, namely, an accurate calibration of the retrofitted models incorporating non-opaque building elements and infiltration scenarios, while providing considerable improvements in computational performance. The methodology is denoted as 'Augmented Ensemble Calibration'. Finally, the paper also shows that the proposed augmented methodology results in more accurate Ensemble models, when glazing and infiltration ECMs are considered, compared to the Ensemble Calibration approach, which are directly linked to the additional retrofit functions associated with Augmented Ensemble Calibration.

1.4 Structure of the current paper

The current paper is structured as follows: Section 2 provides background information on the Ensemble Calibration methodology and the effects of model parameter sensitivity on Ensemble Calibration. Section 3 describes the new Augmented Ensemble Calibration methodology, introduced to include glazing and infiltration parameters in the Ensemble Calibration framework. First, glazing parameters are added using functional extensions of the existing

Ensemble model. Then, a simplified modelled infiltration model is introduced to emulate the reduction of the infiltration rate due to the addition of ECMs. Section 4 demonstrates, from a numerical perspective, the suitability of the proposed method as a computationally efficient, yet accurate method to incorporate the thermal effects of glazing and infiltration reduction using the Augmented Ensemble Calibration framework. Section 5 provides a discussion and conclusions.

2. Background

2.1 Ensemble Calibration

Lumped-parameter building models are linear representations of heat balance in the building. The approach is based on the electric analogy method introduced by Robertson and Gross (1958). The resistances and capacitances of the electric circuit represent thermal resistances and capacitances of material layers in a building element. The model is simplified by lumping parameters together, hence the name of the method. One topology firmly established in the literature is the 3R2C model (Lorenz and Masy 1982; Crabb, Murdoch, and Penman 1987). The 3R2C model structure is shown in Figure 1. The model consists of two thermal resistances (R_a and R_b) which represent the thermal resistance between the outdoor environment (T_{amb}) and the room temperature (T_r). The capacitances C_w and C_a represent the thermal capacitance of the envelope and the air mass, respectively. The resistance R_{win} models the glazing thermal resistance (which is the inverse of the glazing thermal transmittance U_{win}).

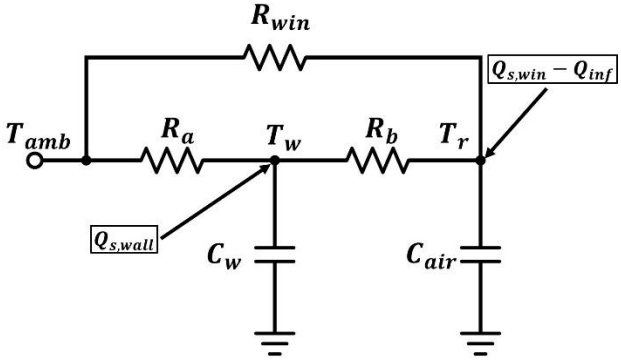

Figure 1. Simplified Lumped Parameter Building Model (3R2C)

Using a semi-physical interpretation of the model structure, it is known that the thermal resistance of the envelope R_a will increase when wall insulation is progressively added. Therefore, the building model parameters can be split into two sets: a set of fixed parameters F, (e.g., baseline model parameters that are not affected by ECMs) and a set of variable parameters V (e.g., the ones that alter due to ECMs). For example, the external wall resistance R_a would be affected by external insulation, thus this parameter belongs to the set of variable parameters V. Thus, all other parameters (i.e., R_b, R_{win}, C_w and C_{air}) belong to the fixed parameter set F. Previous work of the authors (Andrade-Cabrera et al. 2017) demonstrated that the parametric growth of a lumped parameter model can take the shape of an exponential curve. The parametric growth curves can be identified using a sequential optimisation approach. First,

synthetic temperature and heating load time series are generated for the pre-retrofit building and a number of retrofit scenarios (in this case 30 increments of external insulation in 10 mm steps). This synthetic data is obtained using a detached house archetype modelled in the EnergyPlus simulation environment (Neu et al. 2013). The pre-retrofit building model is calibrated using the methodology described in Andrade-Cabrera et al. (2016). Then, a local optimisation is performed using a gradient descent solver, which requires the determination of an initial point. For each increment in insulation, the calibrated external resistance R_a is re-calibrated. In this case, the optimal pre-retrofit resistance $R^{\star}_{a_0}$ is used as the first initial point. During the first iteration, the objective is to calibrate the resistance R_a when $\Delta x_{ext} = 10\ mm$. This optimally calculated value, denoted $R^{\star}_{a_{10}}$ is the initial value of the second iteration. The second iteration calibrates the resistance R_a when $\Delta x_{ext} = 20\ mm$ (i.e., $R^{\star}_{a_{20}}$) using $R^{\star}_{a_{10}}$ as the initial point. The procedure is repeated for each insulation increment. Figure 2 shows that, for each iteration, the annual average internal temperature increases (Figure 2a), while the Energy Use Intensity (EUI) (Figure 2b) decreases as insulation thickness increases. The gradient descent solver compensates for these simultaneous variations by means of increasing the identified value of the calibrated external resistance R_a, thus resulting in a parameter growth curve (Figure 2c).

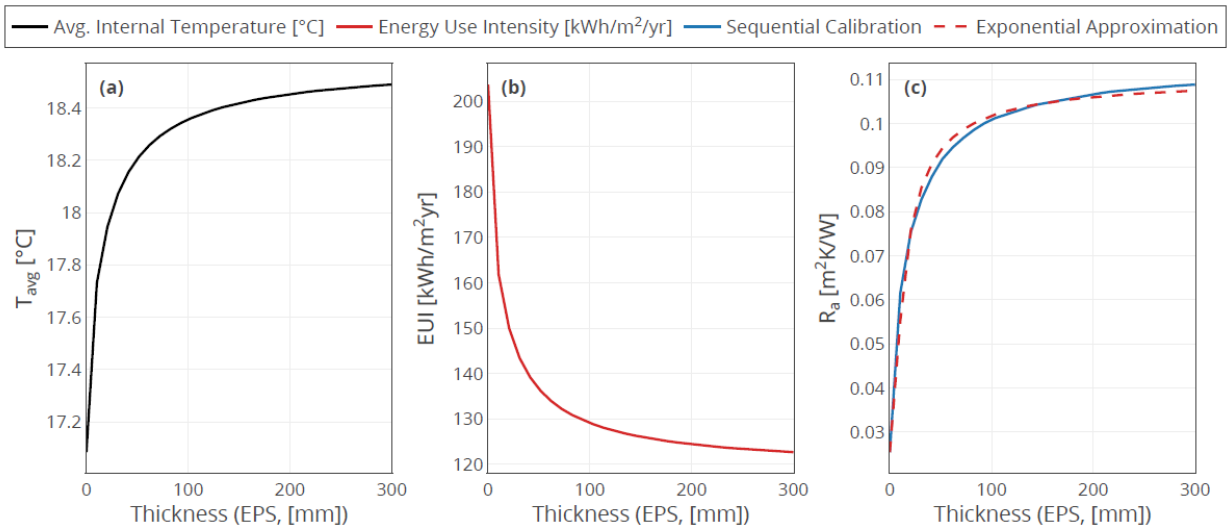

Figure 2. Evolution of Average Internal Temperature (a), Energy Usage Intensity (b) and Calibrated External Resistance (c) as a function of insulation thickness

Note that the calibrated external resistance values shown in Figure 2c are not relatable to the resistance values expected in building elements (e.g., external wall resistance being the inverse of wall U-Values). The model parameters (e.g., thermal resistances and capacitances) have been identified using an automated calibration algorithm based on random initialisation and parameter evolution (i.e., PSO). Thus, the calibrated values of modelled element resistances and capacitances will alter reciprocally during model calibration, as they are related by the products $R_x C_y$. The model remains semi-physical in the meaning of the parameters, but the numerical values of these parameters are likely to diverge from white-box models

The exponential approximation of the evolution of the calibrated external resistance (Figure 2c) is denoted *retrofit function* The retrofit function of R_a takes an exponential form, which can be approximated using the relationship;

$$R_a\left(\Delta_{x_{ext}}\right) \simeq R^{\star}_{a_0} + \alpha_{ext} e^{(1-\beta_{ext})\Delta x_{ext}},\ \ \Delta x_{ext} \geq 0 \qquad (1)$$

that is, the external resistance R_a is a parametric function of the insulation thickness Δx_{ext} and the optimally calibrated parameter for the baseline lumped model parameter $R^{\star}_{a_0}$ (i.e., the parameter corresponding to the model prior to ECMs). Previous work (Andrade-Cabrera et al. 2017) demonstrated that both the baseline lumped parameter and the retrofit function (Equation 1) must be identified at the same time as the calibration parameters α_{ext} and β_{ext}.

Figure 2 corresponds to a scenario where external insulation has been considered as the only ECM implemented in the dwelling. Thus, other building retrofit measures are not considered and thus not modelled (e.g., high air leakage rate, thermally inefficient windows, uninsulated ceiling). The increment in room temperature is marginal because of the existence of a thermostatic controller set to 18 °C. More importantly, the reduction in EUI is not as significant as would be expected (given the investment required in external wall insulation) because of the thermal losses through other building elements. Hence the need to calibrate building models for additional ECM configurations. Ensemble Calibration enables researchers to simultaneously calibrate a baseline (i.e., pre-retrofit) building model and the retrofit functions which represent a number of pre-defined ECM configurations.

The current paper addresses a previously shown limitation of the Ensemble Calibration method, which is the unsuitability of defining glazing and infiltration parameters as retrofit functions due to their effect on the error cost function and the discontinuous nature of discontinuous, unevenly spaced glazing and infiltration retrofit scenarios.

3. Methodology

3.1 Methodology overview

The methodology framework is described in Figure 3. First, the building modelling assumptions and the definition of the ECMs considered in the current paper are described in Section 3.2. In addition, the two modelling limitations associated with the Ensemble Calibration method are outlined. Section 3.3 explains the reasons why parameters that have high indexes of sensitivity with respect to the calibration cost function (such as glazing parameters) cannot be directly implemented in an Ensemble Calibration Framework. Next, a simplified infiltration reduction model is defined in Section 3.4. The model, described in the ASHRAE Fundamentals book (ASHRAE 2017), approximates the percentage of air leakage reduction associated to each building envelope element. The model is augmented with empirical results from Hong et al. (2004) for the case of cavity walls. This infiltration model improves the representativeness of Ensemble Calibration models with respect to building performance post ECM installation.

Section 3.5 describes the *Augmented Ensemble Calibration* approach, which is a crucial stage needed for the use of models obtained through the Ensemble Calibration methodology in scenarios that are representative of retrofit practice. This additional stage enables the incorporation of glazing information in an Ensemble Calibration framework using

an augmentation mechanism, while incorporating a customized infiltration model to account for discontinuous improvements in airtightness due to the installation of ECMs. The algorithm requires as an input an Ensemble Calibration model. It will be shown that the Augmented Ensemble Calibration methodology results in greater calibration accuracy and faster computational times when compared to the equivalent Ensemble Calibration problem.

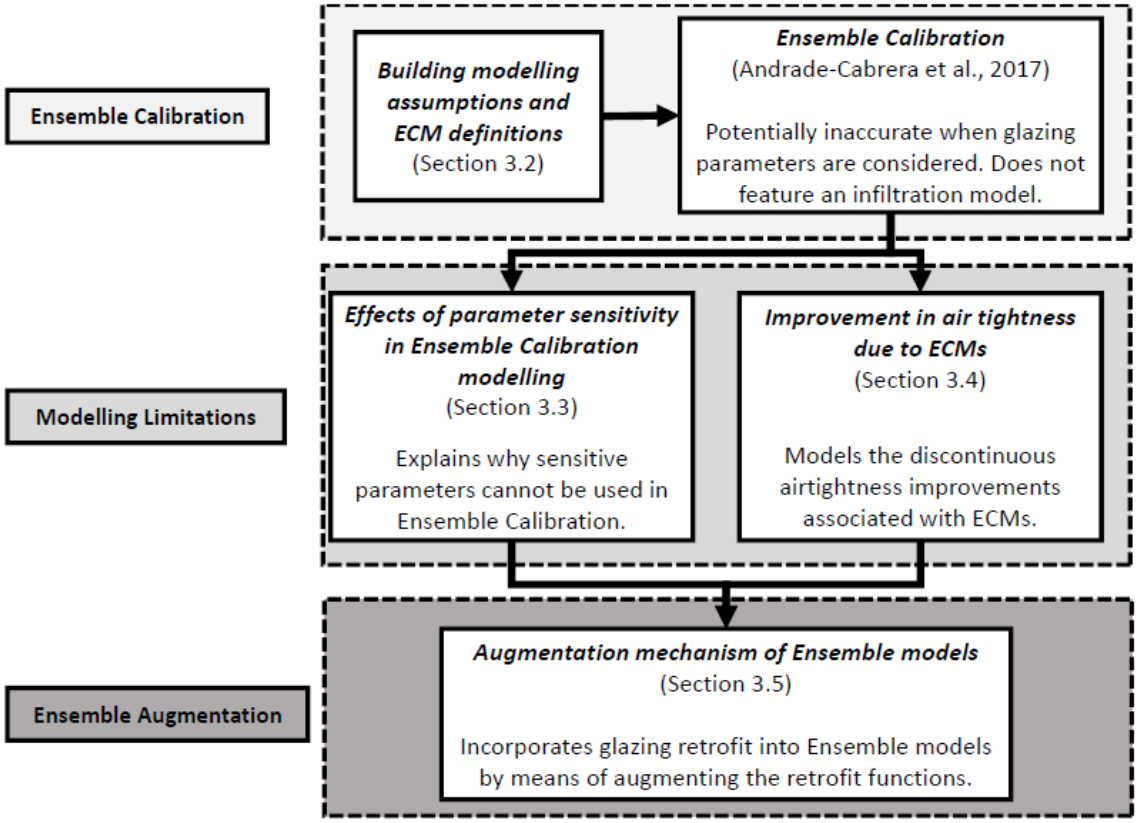

Figure 3. Overview of the proposed methodology

3.2 Building modelling assumptions and ECM definitions

The work in the current paper focuses on the lumped parameter building modelling and calibration of an EnergyPlus detached house archetype model representative of houses built in Ireland before 1990 (Neu et al. 2013). The original archetype was modelled with double-glazed windows (u_{win} = 3.2 W/m^2K, g_{win} = 0.759), heavy solid wall construction (U_{value}=2.27 W/m^2K), a roof (U_{value} = 6.3 W/m^2K) and a moderate infiltration rate (0.6 ACH). Each of the 13 thermal zones is heated with direct electric resistance heaters. Figure 4 shows the proposed 9R6C heterogeneous lumped parameter building model topology associated with this archetype. The average room temperature (T_r) is an area-weighted average of the heated zones. Nodes C_{w1} and C_{w2} model the outer and inner leaves of the external walls. The solar gains due to solar radiation on the walls, $Q_{s,wall}$ are applied directly to node C_{w1}. C_a represents the capacitance of the room air mass with room temperature T_r. Node C_{int} captures the thermal mass of the internal partitions and other slow dynamics. The window solar heat gain $Q_{s,win}$ and the heating power input Q_{heat}

are split between C_a and C_{int} via parameters f_1 and f_2. Node C_{ceil} models the ceiling between the room node C_a and the attic node C_{attic}. The solar gains due to incident solar radiation on the roof surfaces $Q_{s,roof}$ are applied to the roof node C_{roof}. Finally, the ground node C_{gnd} is added to model the heat transfer between the conditioned air volume and the foundations. The temperature T_{gnd} models the temperature under the conditioned air volume (boundary condition 'Ground' in EnergyPlus). The building does not feature an attic zone, as the attic space is ventilated and considered to be in thermal equilibrium with the ambient outside during the heating season. Therefore, the attic temperature T_{attic} is extracted from EnergyPlus. This simplification enables the analysis of the proposed methodology without the additional complexity of modelling the dwelling as a two-zone dwelling. Weather conditions correspond to the Dublin IWEC 2 weather file (ASHRAE 2012).

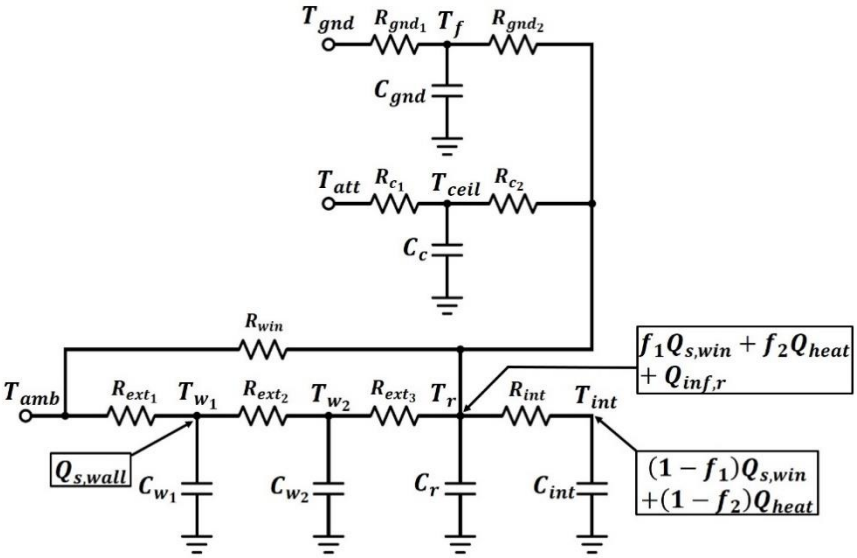

Figure 4. Lumped-parameter building model topology for detached house

The heating schedule is defined by two availability periods: one in the morning (7AM to 9AM) and another in the evening (5PM to 11PM). Outside of these availability periods, the heating does not operate. The temperature set-point is deemed to be 21°C for living areas and 18 °C for all other thermal zones. These set-points and schedules are representative of domestic heating requirements in Ireland (AECOM 2013). Since one of the rooms was designated as a living space, the effective set-point of the combined single zone, after area weighting, is 18.3 °C. The resulting network topology is identical to the model introduced in the previous study, which dealt with semi-detached house modelling (Andrade-Cabrera et al. 2017). However, the detached house archetypes include solar radiation on all possible facades, whereas in the semi-detached house modelling, the south façade was modelled as adiabatic both in the lumped parameter model and in the EnergyPlus archetype model, in order to emulate the presence of an adjacent property. A room air mass capacitance multiplier of 11 has been introduced to emulate slower dynamics in the thermal dwelling which are more representative of domestic dwellings (Greensfelder, Henze, and Felsmann 2011). Without the multiplier, the thermal response of the dwelling (i.e., the weighted average temperature) rapidly increases or

decreases after the heating systems are turned on or off, respectively. Internal gains and ventilation losses (i.e., ventilation losses other than infiltration) are ignored for calibration purposes (i.e., they are removed from the source archetype). However, these heat gains or losses can be added later as heating gains in a co-optimisation scheme.

Table 1 describes the ECM measures studied in the current paper. The ranges for the ECM measures were suggested in the Cost-Optimal Calculations and Gap Analysis study for the Irish residential stock (AECOM 2013), which was used as a primary information resource for the modelling of the archetypes used in the current work (Neu et al. 2013). Table 1 also states the parameters that are deemed to be variable and therefore, functions of monotonically increasing ECM measures. The insulation measures are associated with an Ensemble index. These indexes are used for a proposed hand notation $\{M,N,O,P\}$ which describes ECM configurations models without a lengthy technical description. The indexes M, N and O describe an increment in external, internal and ceiling insulation. An index value of 1 represents no retrofit measure (and thus the variable parameter is equal to the parameter of the baseline model), whereas an index value of 4 indicates the maximum retrofit value (e.g., 300 mm for ceiling insulation). The current paper introduces index P as a metric which represents discontinuous increments in thermal glazing performance due to the replacement of poorly performing glazing by higher efficiency glazing. Tailored airtightness ECMs can be incorporated into the Augmented Ensemble Calibration framework. However, they are not considered in the current paper for the reasons described in Section 3.4. Installing 300 mm of external wall insulation is not a common ECM from an installation constraint perspective. However, this ECM must be included for the calculation of the retrofit function (Equation 1) which results in external wall insulation ECMs with thicknesses of 100 mm and 200 mm.

Synthetic building performance data was generated for every possible ECM configuration, with the exception of configurations where there would be combined internal and external insulation measures, as the application of simultaneous external and internal insulation of an external wall would not be sensible in retrofit practice. This exception reduces the number of ECM configurations to 112 in lieu of 256 configurations (i.e., 4^4 configurations). An automated script was developed to alter the pre-retrofit detached house archetype EnergyPlus model and extract the relevant performance data (namely, the average weighted air temperature $T_{r,data,}$ and the total heating load $Q_{,heat,data}$).

Index	*Insulation*	*Units*	*1*	*2*	*3*	*4*	*Parameter*
M	External Insulation (EPS)	mm	0	100	200	300	R_{ext_2}
N	Internal Insulation (EPS)	mm	0	50	100	150	R_{ext_3}
O	Ceiling Insulation (Glass wool)	mm	0	100	200	300	R_{ceil_2}
$P\{$	Window Replacement (U_{win})	W/m^2K	3.2	1.6	1.4	0.9	U_{win}
	Window Replacement (g_{win})	-	0.79	0.73	0.73	0.6	g_{win}

Table 1. ECM measures and associated parameter range

3.3 Effects of parameter sensitivity *in Ensemble Calibration modelling*

A standard Particle Swarm Optimisation (PSO) algorithm, while allowing for a wider search in the solution space, is also known to attract the solutions (i.e., the particles) to the upper or lower boundaries (Hassan and Cohanim 2005). This behaviour can potentially result in an aggressive calibration of building energy model parameters representative of fast building thermal response and therefore, in a potential loss of calibration accuracy. The PSO algorithm minimises the performance error between the building models and the synthetic data by means of determining the best particle (i.e., the optimally calibrated model) at each iteration until the PSO algorithm converges. The individual model cost function becomes the Root Mean Square Error (RMSE) over the calibration horizon, that is:

$$J\big(p(i,l)\big) = \sqrt{\frac{\sum_{k=0}^{k=NH}\left(T_{r,data,k} - \mathrm{T_{r,k}}(i,l)\right)^2}{NH}} \tag{2}$$

where $p(i,l)$ represents the position (i.e., the model parameters) of the candidate particle i at optimisation time-step l. NH represents the calibration horizon. $T_{r,data,k}$ corresponds to the synthetic temperature time series used for calibration, and $\mathrm{T_{r,k}}(i,l)$ is the room temperature obtained from the model response. Using the $RMSE$ as the cost function accounts for large error deviations due to the squaring of large temperature deviations at a given time step. The Ensemble Calibration algorithm calculates the cost function for each model being considered (i.e., each desired ECM configuration) and sums the individual cost functions in a *global* cost function. The Ensemble Calibration algorithm aims to minimise this global cost in order to find baseline model parameters and retrofit functions that are representative of all the models. The Particle Swarm Optimisation works in a manner such that the particles are attracted to the best possible solution in the entire swarm and the best particle in the neighbourhood (i.e., a cluster of particles randomly grouped at each PSO iteration). The current paper uses a standard implementation of the PSO algorithm (Mathworks 2015). In this algorithm, the particles are constrained by upper and lower boundaries. If an element of the particle (e.g., a glazing parameter) exceeds the boundary, then it is defined at the boundary for numerical evaluation purposes. Therefore, it is possible that large variations in highly sensitive parameters, will result in the largest improvements in the early stages of Ensemble Calibration at the expense of identifying model parameters at the boundary and ultimately resulting in an inaccurate calibration for all models.

A sensitivity analysis of the variable parameters of the model was carried out using the analysis tools developed by Marino et al (2008). Figure 5 shows the calculated Partial Rank Correlation Coefficients ($PRCC$) of the building model parameters with respect to the calibration error function (i.e., the $RMSE$ between the model response and the surrogate data). A positive $PRCC$ value indicates a positive correlation whereas a negative PRCC value corresponds to a negative correlation. A $PRCC$ of 0 means that there is no correlation with respect to the error function whereas a value of ±1 implies perfect correlation. The Ensemble Calibration framework defines model parameters as either fixed (i.e., not affected by ECM options) or variable (i.e., parameters that will evolve when increments in the selected ECM occur). The thermal resistances are considered as variable parameters as they would be expected to increase when insulation measures are installed in the opaque envelope. The thermal capacitances are deemed as fixed to the

default theoretical values. Furthermore, the infiltration parameter ACH_{inf} and the glazing parameters U_{win} and g_{win} are deemed as variable parameters.

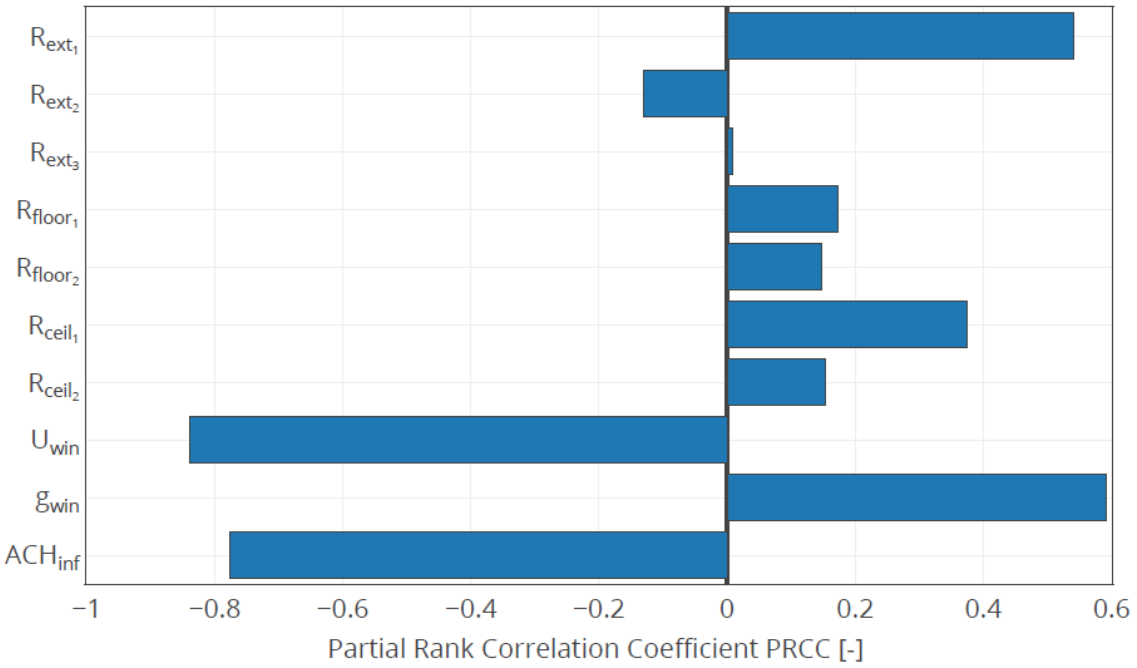

Figure 5. Partial Rank Correlation Coefficient (PRCC) of the calibration function ($RMSE$) with respect to the building model parameters of the 9R6C topology shown in Figure 4

The previous study (Andrade-Cabrera et al. 2017) concluded that using R_{ext_1} (i.e., the external wall resistance subject to ambient conditions) as a variable parameter was not an appropriate choice. Figure 5 shows that the calibration error function is very sensitive to variations in R_{ext_1} ($PRCC$ = 0.541). Therefore, when R_{ext_1} was allowed to vary (and thus was associated with a retrofit function), the Ensemble Calibration algorithm had to: (a) identify the baseline parameter R_{ext_1} and, (b) identify the functions that map all possible scenarios of R_{ext_1} for all possible ECM configurations. This implies that, in practice, all models vary significantly as R_{ext_1} varies and thus a sub-optimal calibration was obtained. However, in the case of wall insulation, it is possible to express the variation of wall thermal transmittance (U_{wall}) by the relationship:

$$U_{wall} = \frac{1}{\left(\mathrm{R}_{\mathrm{ext}_1} + \mathrm{R}_{\Delta x_{ext}}\right) + \mathrm{R}_{\mathrm{ext}_2} + \mathrm{R}_{\mathrm{ext}_3}} = \frac{1}{\mathrm{R}_{\mathrm{ext}_1} + \left(\mathrm{R}_{\mathrm{ext}_2} + \mathrm{R}_{\Delta x_{ext}}\right) + \mathrm{R}_{\mathrm{ext}_3}} \quad (3)$$

Therefore, it is possible to use $\mathrm{R}_{\mathrm{ext}_2}$ as a surrogate variable to capture the variation in thermal performance of the building envelope due to the addition of external insulation, while keeping the same thermal transmittance. However, building model parameters representative of fast thermal response such as window thermal transmittance U_{win} ($PRCC$ = -0.838), window solar transmittance g_{win} ($PRCC$ = 0.591) and the infiltration rate ACH_{inf} ($PRCC$ = 0.831) cannot

be modelled using a surrogate parameter. Therefore, a new methodology is required to incorporate window and infiltration retrofits in the Ensemble Calibration framework.

3.4 Improvement in air tightness due to ECMs

The introduction of ECMs results in secondary energy savings due to the increase in air tightness. This effect occurs due to the covering of cracks and the reduction in the overall porosity of the retrofitted building envelope. Up to 70% of infiltration airflow enters a building diffusely via cracks in the envelope (Sinnott 2016). Hong et al. (Hong, Oreszczyna, and Ian 2004) proposed an air leakage reduction model where the air leakage reduction is decomposed by building elements using a regression analysis from field data. The model identified results comparable to Kinnane et al. (2016) (i.e., 24% reduction in air leakage reduction) under a similar retrofit scenario (cavity insulation and draught stripping). The model suggests that ceiling (loft or attic) insulation contributes 14% to air leakage reduction, whereas draught stripping alone contributes to 5% and window replacement (post-draught proofing) contributes an additional 3% reduction in air leakage (since draught stripping measures were assumed to be already in place).

In the Irish context, Sinnott (2016) carried out experimental measurements of air leakage post and pre-retrofit. Sinnott found an average reduction of 25.6% in air leakage post-retrofit for two-storey residential buildings. The retrofit measures consisted of a mixture of cavity insulation, attic insulation and draught proofing measures alongside other systems and envelope upgrades. In (Gillott et al. 2016), a number of air tightness measures were progressively made and infiltration tests were taken as retrofit measures were progressively added. It was found that draught proofing and sealing of the floor/wall joint provided reductions in air permeability of 5.73 and 3.6 $m^3/hr/m^2$, respectively. However, such findings are specific to a single dwelling and they would be difficult to reproduce at scale. Moreover, the effectiveness of specific retrofit measures (e.g., envelope sealing) are properties of the individual dwellings.

The current paper adopts estimates of air leakage of building components described in the ASHRAE Handbook of Fundamentals (ASHRAE 2017). These estimates are based on the findings of Dickerhoff et al. (1982). External walls contribute between 18% to 50% of air leakage, with an average of 35%. Ceilings contribute between 3% to 30% of air leakage, with an average of 18%. Finally, windows and doors represent between 6 to 22% of air leakage, with an average of 15%. The study by Dickerhoff et al. does not explicitly state the percentage of air leakage reduction associated with cavity wall insulation. Cavity wall insulation is often carried out with porous materials and therefore it is reasonable that a full surface measure (i.e., wall insulation) would reduce the infiltration rate at a higher rate. The current paper will use an estimate of 11% of reduction in air leakage post cavity wall retrofit. This value is adopted from the model described by Hong et al. (2004). While the findings reported in Dickerhoff et al. correspond to American constructions (e.g., timber frame walls), which may differ from European constructions (e.g., masonry walls), these estimates will be adopted in the absence of an equivalent study for European constructions.

Numerically, the proposed air tightness reduction model is implemented as a parametric equation:

$$\overline{ACH_{inf}} = \left(ACH_{inf,0} - ACH_{inf,ECM}\right) \times \left(1 - \sum_{n=1}^{n_\kappa} f_{inf,n}\,\kappa_n\right) \quad (4)$$

where $ACH_{inf,0}$ is the baseline infiltration rate, $ACH_{inf,ECM}$ represents the reduction in airtightness due to a tailored ECM (e.g., window/door stripping - also opaque measures), and $f_{\text{inf,n}}$ is a fractional parameter which reduces the modelled infiltration rate, if a given ECM measure κ_n is selected. The fractional parameter and the corresponding modelled infiltration rates are defined in Table 2. Only five ECM configurations are considered (n_κ=5). Table 2 also describes the modelled infiltration after individual measures are included. The baseline infiltration case (0.67 ACH) is used for demonstration purposes. Note that the modelled infiltration will significantly reduce after multiple ECMs are combined. For example: adding wall insulation, ceiling insulation and window replacement will result in a 68% reduction of the infiltration rate, that is a reduction in the modelled infiltration rate from 0.67 ACH to 0.26 ACH.

κ	*Configuration*	*Associated* $f_{inf,n}$	*Modelled infiltration* ACH
κ_1	Baseline model	0.00	0.67
κ_2	Wall Insulation	0.35	0.44
κ_3	Ceiling Insulation	0.18	0.55
κ_4	Cavity Wall Insulation	0.11	0.60
κ_5	Window Replacement	0.15	0.56

Table 2. Fractional percentage of infiltration rate reduction associated with each ECM measure

3.5 Augmentation mechanism of Ensemble models

The current paper introduces a mechanism to incorporate window retrofits into the Ensemble Calibration framework. The mechanism consists of the augmentation of the retrofit functions of a pre-computed Ensemble model (e.g., Equation 1) with auxiliary functions which model the variations in building thermal dynamics due to window upgrade. For example, the variations of lumped model parameter R_{ext_2} as external wall insulation is progressively added, can be modelled using the retrofit function:

$$R_{ext_2}\left(\Delta_{x_{ext}}\right) \simeq R^{\star}_{ext_{2,0}} + \alpha_{ext} e^{(1-\beta_{ext})\Delta x_{ext}}, \quad \Delta x_{ext} \geq 0 \quad (5)$$

The augmentation algorithm enhances the function with the additional terms:

$$R_{ext_2}\left(\Delta_{x_{ext}}\right) \simeq R^{\star}_{ext_{2,0}} + \alpha_{ext} e^{(1-\beta_{ext})\Delta x_{ext}} + \mu_{ext} e^{(1-\nu_{ext})\Delta x_{ext}}, \quad \Delta x_{ext} \geq 0 \quad (6)$$

where μ and ν are calibration parameters that model the augmented parametric growth function. As in Ensemble Calibration, the current paper models the parameter augmentation function as an exponential function. The Augmented Ensemble Calibration procedure is described in Appendix A. The algorithm requires, as input, a calibrated Ensemble model. That is, the augmentation algorithm requires as input the Ensemble baseline parameters p_0 and the pre-computed Ensemble function parameters calculated prior to augmentation (e.g., $\alpha_{ext,M,O}$). The Augmented

Ensemble Calibration algorithm assumes that the same configuration of fixed parameters (F) and variable parameters (V) are partitioned in the preliminary Ensemble calibration step. The set of variable parameters under augmentation, denoted as $\overline{V_P}$, includes the same parameters listed in V. The sub-index P is defined as the Ensemble index for glazing measures. Hence $\overline{V_P}$ denotes the set of parameters after window retrofits.

The Augmented Ensemble Calibration algorithm makes assumptions on the pre-retrofit parameters for window thermal transmittance $u_{win,0}$, window solar transmittance $g_{win,0}$ and infiltration rate ACH_0. Since the baseline parameters $p_0^\star$ and the Ensemble function parameters (e.g., α_{ext}, β_{ext}) are precomputed, they are deemed to be constant. Therefore, the particle $p(i)$ includes only the variable parameters under augmentation (i.e., $\bar{V}$). This implies the definition of upper and lower boundaries for the dimensionless augmentation growth parameters (e.g., μ_{ext} and ν_{ext}). In the current paper, the upper and lower bounds for the augmentation growth parameters are defined as 0.01 and 2, respectively. These tuning parameters need to be determined by the building modeller until the desirable performance is reached. When an opaque ECM measure is considered, the appropriate parameter growth equation (Equation 2) is applied. Then, the continuous time model is computed, discretised and the local cost function is evaluated. In Augmented Ensemble Calibration, the cost function is the root mean square error ($RMSE$) between the surrogate data and the model response (Equation 2). As in Ensemble Calibration, the global cost function is updated. The global cost is the sum of all the local particle costs, thus enabling the PSO algorithm to identify solutions which simultaneously reduce the performance error (i.e., the cost) for all of the models. The procedure iterates until the model converges. The standard PSO algorithm, used in this work (Mathworks 2015), was configured to converge after the relative change in the optimal cost function at the optimisation time-step l is less than 0.001 K during 20 consecutive iterations.

4. Results and Discussion

4.1 Overview

The results section is organized as follows: Section 4.2 shows the results of the implementation of the Ensemble Calibration methodology using the building model and ECM configurations described in Section 3.2. These results demonstrate the current capabilities of the Ensemble Calibration method (i.e., the models can only be accurately calibrated if glazing retrofit is disregarded). Section 4.3 shows the results of Ensemble Calibration when the infiltration model (Section 3.4) is incorporated. While the infiltration model is meant to be used as part of the Augmented Ensemble Calibration algorithm (Appendix A), a comparison between Ensemble Calibration and Augmented Ensemble Calibration can only be done if both algorithms feature the infiltration model. Section 4.3 shows a slight improvement in accuracy for the retrofitted models as a result of the reduction in airtightness.

Section 4.4 demonstrates the underperformance associated with Ensemble Calibration when glazing parameters are considered as variable parameters (i.e., modelled as retrofit functions). It is shown that, as discussed in the Introduction, the glazing parameters are attracted to the boundary values and thus the calibration accuracy is

undesirable. Section 4.5 describes the results obtained using the Augmented Ensemble Calibration. The algorithm results in an accurate calibration of the building models featuring glazing retrofits. Section 4.6 describes the computational performance of the proposed calibration algorithms.

Table 3 describes four different ECM configurations which have been selected for testing purposes. The test cases have been selected to represent realistic ECM configurations which may be encountered in practice. Test 1 represents the baseline (i.e., pre-retrofit scenario). Test 2 represents a dwelling with a mixture of external wall and ceiling insulation, and where windows have been upgraded to more energy efficient double-glazed uPVC windows. Test 3 represents a mixture of internal wall and ceiling insulation, with the same glazing as in Test 2. Test 4 explores a scenario which could be found in deep retrofit scenarios, where external wall insulation (100 mm) and ceiling insulation (300 mm) is combined with high performing glazing (triple-glazed uPVC windows).

ECM	*Units*	*Test 1*	*Test 2*	*Test 3*	*Test 4*
External Insulation (EPS)	mm	0	0	0	100
Internal Insulation (EPS)	mm	0	0	100	0
Ceiling Insulation (Glass wool)	mm	0	300	300	300
Window Replacement (U_{win})	W/m^2K	3.2	1.6	1.6	0.9
Window Replacement (g_{win})	-	0.79	0.73	0.73	0.6

Table 3. ECM configurations (Tests 1-4).

Three calibration metrics are considered in this study. The first is the Mean Absolute Error (MAE) which represents the difference between synthetic data and model response. An MAE value below 0.5 K has been defined in the literature as an acceptable value (Kusiak and Xu 2012; He, Zhang, and Kusiak 2014). The second metric is the $RMSE$ value, which is effectively the cost function of the individual model (Equation 2). The third metric is the Mean Biased Error (MBE), which signals whether a model underestimates (positive sign) or overestimates (negative sign) the building thermal response.

4.2 Ensemble Calibration

Figures 6 and 7 show the performance of the Ensemble Calibration procedure applied to the detached house archetype model under the assumptions defined in Section 3.2. The Ensemble Calibration method does not incorporate glazing parameters. Therefore, Figures 6 and 7 represent the calibration of the test cases prior to window retrofit. The Ensemble Calibration model is capable of accurately calibrating the models prior to window glazing retrofit (as expected). Figure 6 shows that the thermal response is accurately calibrated for a selected range of peak heating days (Dec 18th to Dec 28th). Figure 7 describes the performance of the Ensemble Calibration model as Mean Absolute Error histograms. A distribution positively skewed (towards the left) represents a model calibrated with a higher level of accuracy. The models were calibrated using hourly synthetic data for a calibration period of six months (October

15h to 15 March, inclusive). This calibration window captures model performance during the peak heating season (mid-November to mid-March).

Table 2 shows that the test model has been accurately calibrated below MAE = 0.3 K. However, a bias (or penalty) towards the baseline model (Test 1) can be noted (i.e., the error calibration metrics MAE and $RMSE$ are higher for Test 1 than for the other Test scenarios). The global cost function (i.e., the sum of the $RMSE$ of each calibrated model) penalizes the calibration accuracy of the baseline parameter (i.e., the building model prior to retrofits) and a small number of ECM configurations with low levels of insulation because of the larger number of well insulated models being evaluated in the global cost function. Hence the fixed parameters F will be selected in a manner such that the parameters will favour retrofitted model accuracy. The evaluation of alternative cost functions is left outside the scope of the current paper. It could be argued that since the interest is in extracting retrofitted models, a bias on the baseline model can be deemed as an acceptable drawback of the Ensemble Calibration methodology.

Metric	*Test 1*	*Test 2*	*Test 3*	*Test 4*
MAE	0.267	0.253	0.179	0.180
$RMSE$	0.334	0.316	0.235	0.228
MBE	0.512	0.218	-0.021	0.126

Table 4. Performance Metrics for Ensemble Calibration

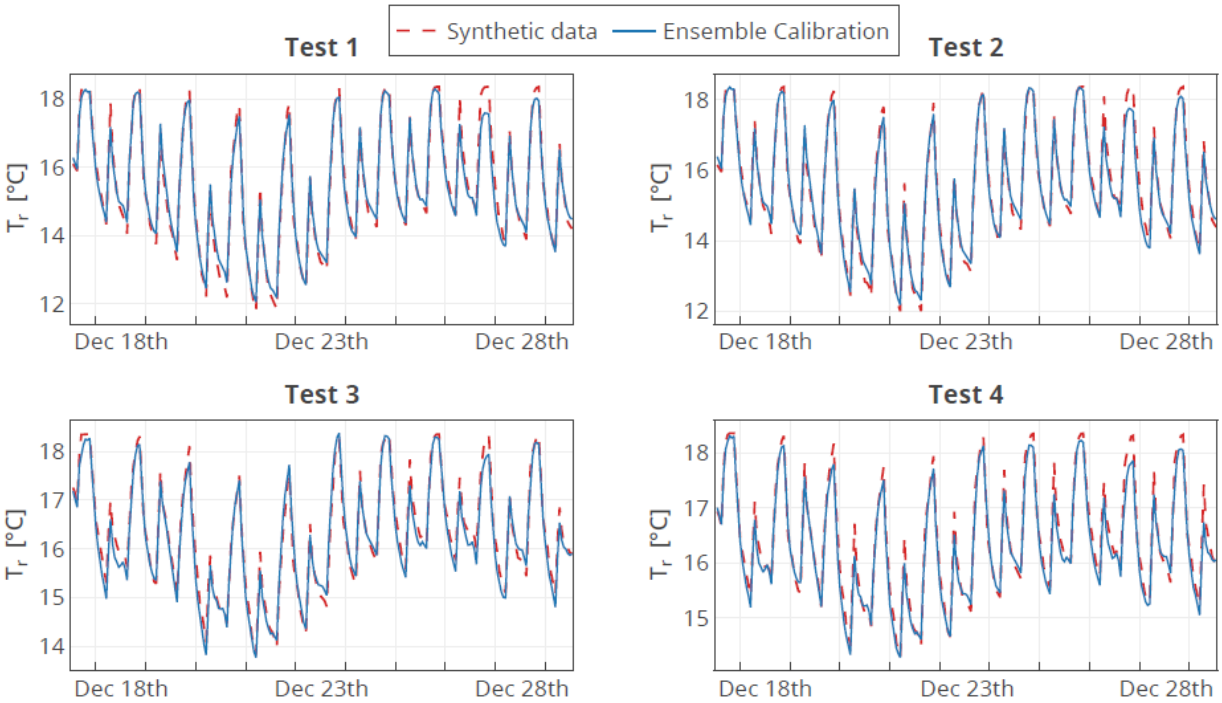

Figure 6. Model Response for Tests 1-4 (Ensemble Calibration)

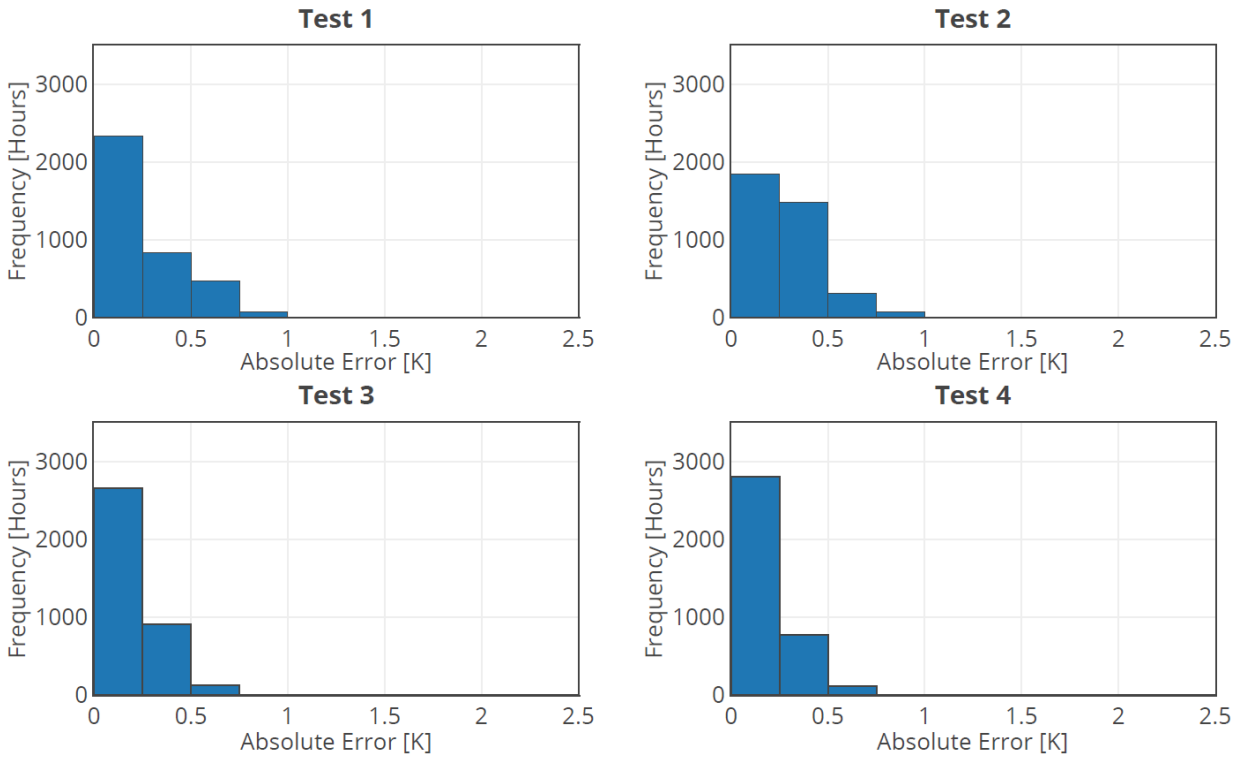

Figure 7. MAE Histograms for Tests 1-4 (Ensemble Calibration)

4.3 Ensemble Calibration incorporating the proposed Infiltration Model

The infiltration model is added to the Ensemble Calibration methodology. Table 5 describes the performance metrics for the Test scenarios. The performance is similar to the performance shown in Table 4 and therefore it can be said that the incorporation of infiltration models in the Ensemble Calibration methodology does not diminish model calibration accuracy. Figure 8 shows the model response and Figure 9 the error histogram of the proposed model after the infiltration model is added. Model accuracy slightly increases for the models with higher insulation as infiltration rates are reduced and therefore, there is a reduced possibility of model mismatch between the calibrated models and the synthetic data.

Metric	*Test 1*	*Test 2*	*Test 3*	*Test 4*
MAE	0.262	0.258	0.174	0.164
$RMSE$	0.325	0.320	0.214	0.205
MBE	-0.030	-0.088	-0.068	-0.009

Table 5. Performance Metrics for Ensemble Calibration with Infiltration model

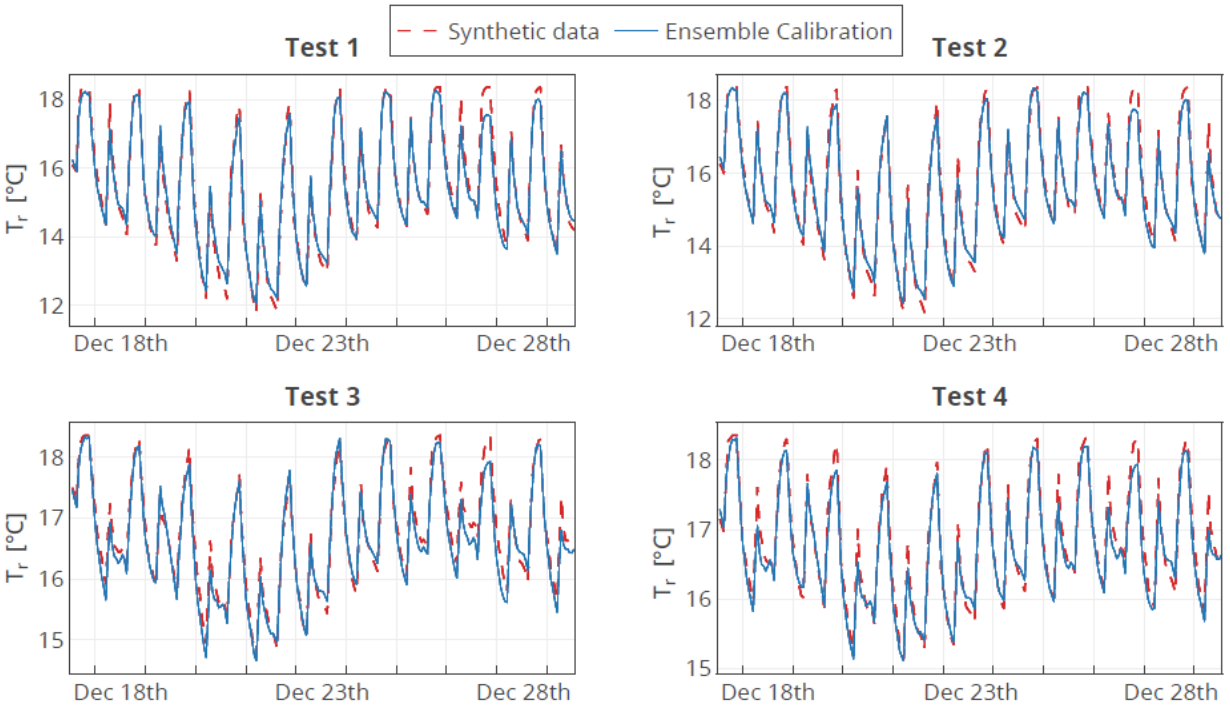

Figure 8. Model Response for Tests 1-4 (Ensemble Calibration with Infiltration model)

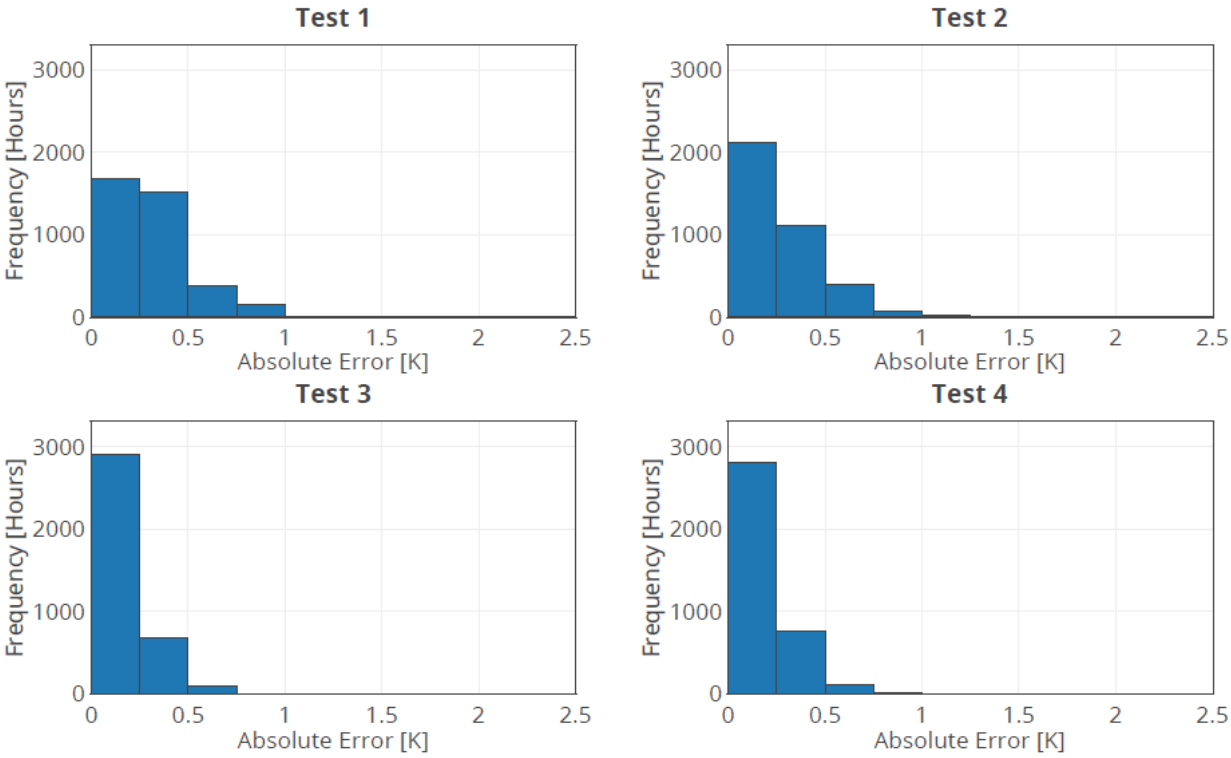

Figure 9. MAE Histograms for Tests 1-4 (Ensemble Calibration with Infiltration model)

4.4 Incorporating glazing parameters as variable parameters

Glazing parameters can be considered as an additional dimension to the Ensemble Calibration procedure. However, the extra glazing terms result in the addition of computational complexity as more dimensions are added to the problem. Most importantly, using glazing parameters as variable parameters results in reduced calibration performance due to model parameter sensitivity. Figure 10 shows the evolution of the glazing thermal transmittance U_{win} for four runs (Calibration 1-4) of the Ensemble Calibration method using the thermal transmittance and the solar transmittance g_{win} as variable parameters. All calibration runs have the same parameters. Thus, the difference in performance between calibration runs is due to the random seed initialisation of the PSO algorithm and the use of normalised random vectors during particle updates (Mathworks 2015). The nominal value of the glazing thermal transmittance pre-retrofit is $U_{win,0} = 3.2\ W/m^2K$. In the Ensemble Calibration framework this parameter is allowed to vary between +/- 25% of the baseline parameter (i.e., 2.4 and 4.0 W/m^2K respectively). In theory, this should allow the Ensemble Calibration method to identify model parameters and retrofit functions which accurately calibrate all possible ECM configurations being considered. Likewise, the nominal value of the glazing solar transmittance pre-retrofit is $g_{win,0} = 0.76$, and it is allowed to vary between 0.57 and 0.95. Figure 10 shows that in three of the calibration runs (Calibration Runs 1 - 3), the identified baseline thermal transmittance parameter $U_{win,0}$ rapidly converges to the upper boundary (e.g., 4.0 W/m^2K) in less than 30 minutes. As discussed earlier, the building model is highly sensitive to the glazing parameters U_{win} and g_{win} (Section 3.3). Therefore, the PSO routine aims to minimise the original cost (i.e., the error between the uncalibrated models and the synthetic data) using the parameters which result in a higher reduction of the global cost function at each iteration. The glazing parameters result in the highest reduction in cost (RMSE) during the earlier iterations because the calibration error function is sensitive to these parameters. Noticeably, $U_{win,0}$ converges faster than $g_{win,0}$ because the calibration function (i.e., $RMSE$) is more sensitive to $U_{win,0}$ ($PRCC$ = -0.831) than to $g_{win,0}$ ($PRCC$ = 0.591) as shown in Figure 5. That is, $U_{win,0}$ has a higher impact on the calibration function and therefore it drives the calibration process. This is exemplified in Calibration Run 1 as $U_{win,0}$ converges to the upper boundary in less than 10 minutes, whereas $g_{win,0}$ converges in approximately 100 minutes (Figure 11).

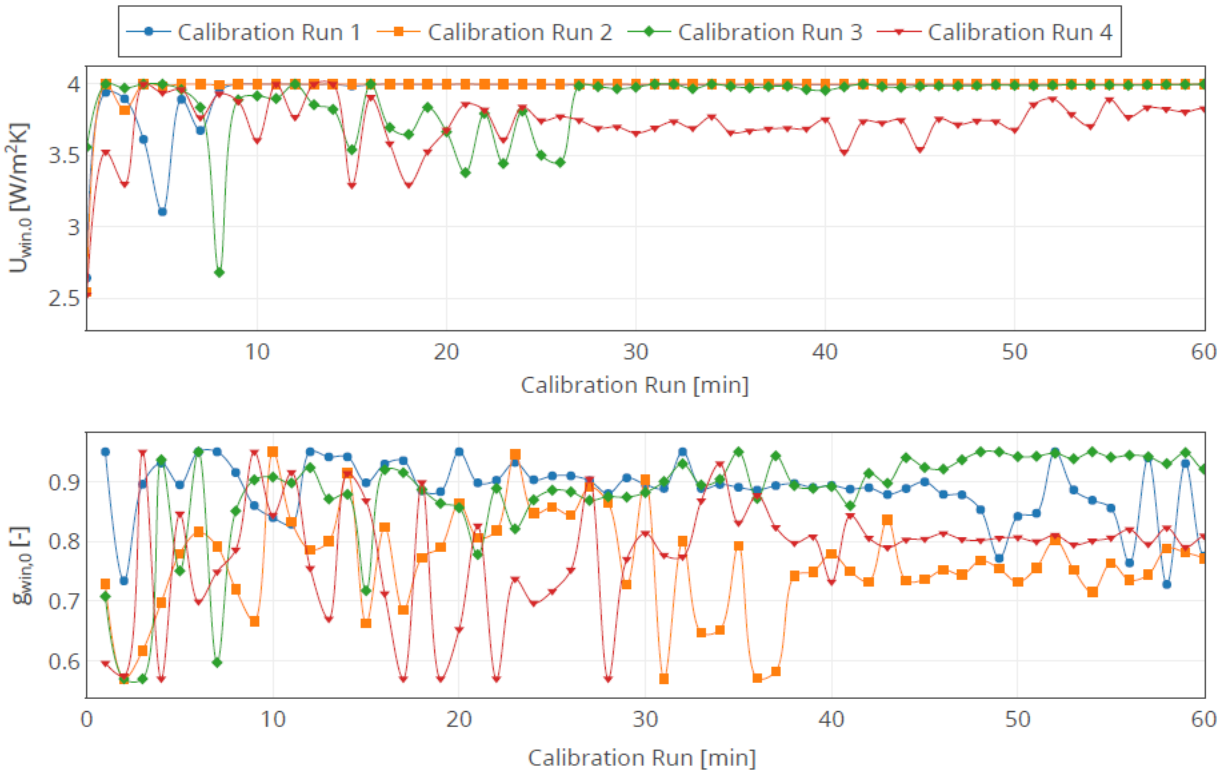

Figure 10. Convergence of effective $U_{win,0}$ and $g_{win,0}$ towards the upper parameter boundary (first hour)

Figure 11 shows that three of the calibration runs (Calibration runs 1, 2 and 4) converge to a sub-optimal solution after approximately 90 min. While Calibration Run 4 is not attracted to the boundary value, it also exits around 1h30m. Calibration Run 3 continues for another 7.5 h after that point. Calibration Run 3 results in a global cost (i.e., the sum of the RMSE of every model, Equation 2) of 19.57 K. This is considerably less than the other calibration runs (e.g., Calibration Run 4 resulted in a global cost of 63.2 K). Therefore, Calibration Run 3 is deemed to be the best candidate calibration obtained using glazing parameters as variable parameters in an Ensemble Calibration framework. The other three calibration runs correspond to scenarios where the algorithm converges to a low-quality solution. The additional time incurred in Calibration Run 3 corresponds to the evolution of the other parameters being calibrated. Hence it is interesting to see that performance switches around 300 minutes (5 hrs). The PSO particles (where each which include all model parameters and retrofit function parameters) continue evolving in a manner such that a better solution is identified at that time and thus $U_{win,0}$ progressively decreases until the calibration run converges to the lower bound (i.e., $U_{win,0} = 2.4\ W/m^2K$).

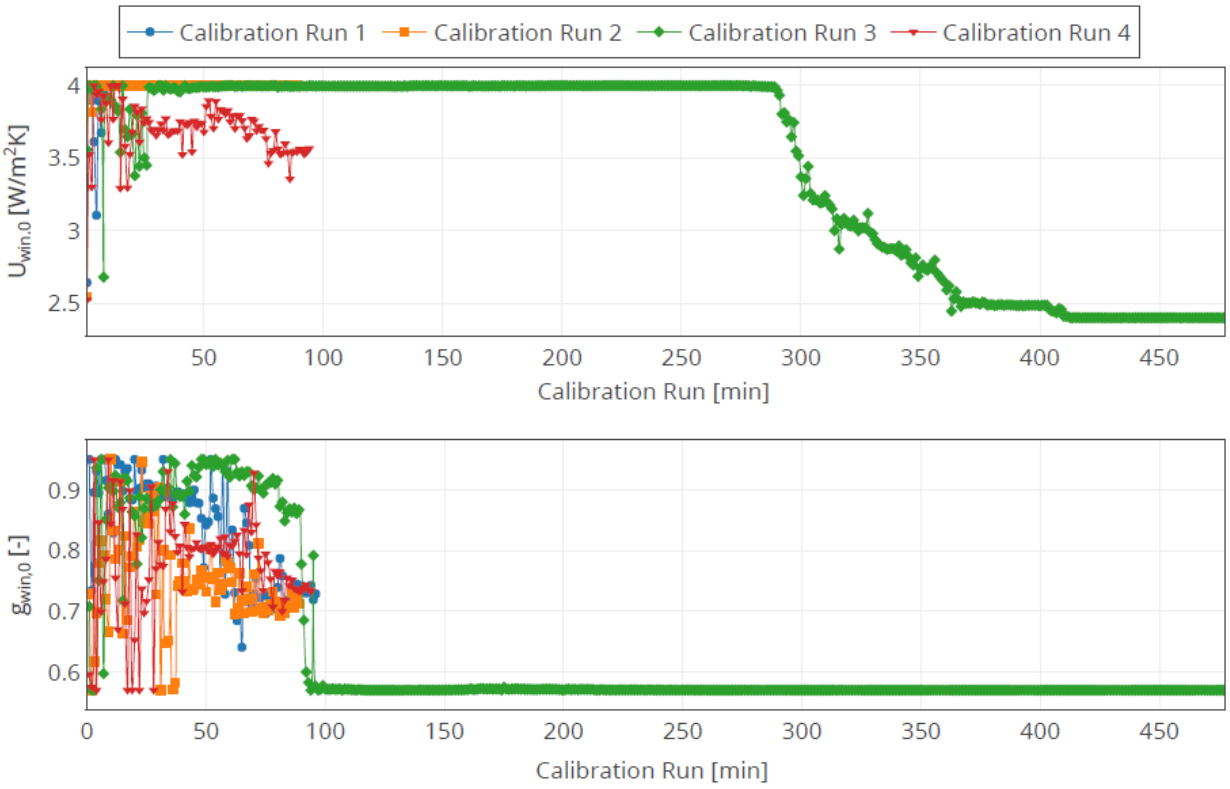

Figure 11. Convergence of effective $U_{win,0}$ and $g_{win,0}$ towards the upper parameter boundary (Entire Calibration Period)

It can be noted that even for the best calibration run (Calibration Run 3) model calibration accuracy is significantly degraded. This issue is illustrated in Table 6. While Tests 2-4 are not directly comparable with Table 4 (i.e., Table 4 does not feature Tests with glazing replacement), the performance metrics should be approximate of equivalent pre-glazing models as shown in Table 4. The insulated scenarios (Tests 2-4) were calibrated with similar levels of accuracy seen in equivalent pre-glazing scenarios. However, Test 1 (which is directly comparable with the metrics in Table 4, as it is the baseline scenario) results in a less accurate calibration. Table 7 shows that the addition of glazing parameters results in a less accurate calibration of the baseline model (MAE = 0.495 K) when compared with the Ensemble Calibration without glazing (MAE= 0.267 K).

Metric	*Test 1*	*Test 2*	*Test 3*	*Test 4*
MAE	0.495	0.519	0.411	0.256
$RMSE$	0.622	0.641	0.506	0.316
MBE	0.889	-0.006	-0.353	-0.106

Table 6. Performance Metrics for Ensemble Calibration using variable glazing parameters

Figures 12 and 13 show that Tests 2-4 present a dynamic performance comparable to the performance seen in Figures 5 and 6 (Ensemble Calibration without glazing parameters). However, Test 1 shows that the data is overestimated. This overestimation is also shown in Table 6 (MBE = 0.889). This underestimation is also noticeable in Figure 13. The MAE distribution for Test 1 is considerably flatter than the distribution shown in Figure 6. Test 3 also shows a slight underestimation of the synthetic data (MBE = -0.353).

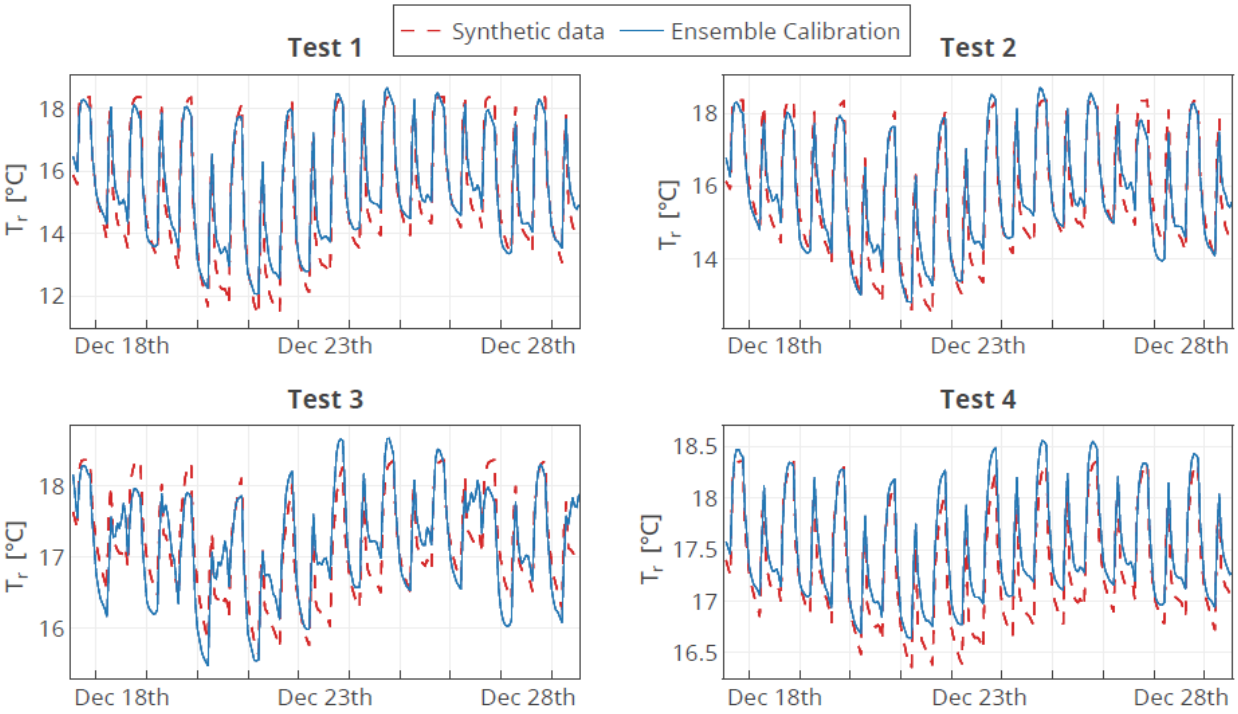

Figure 12. Model Response for Tests 1-4 (Ensemble Calibration with variable glazing parameters)

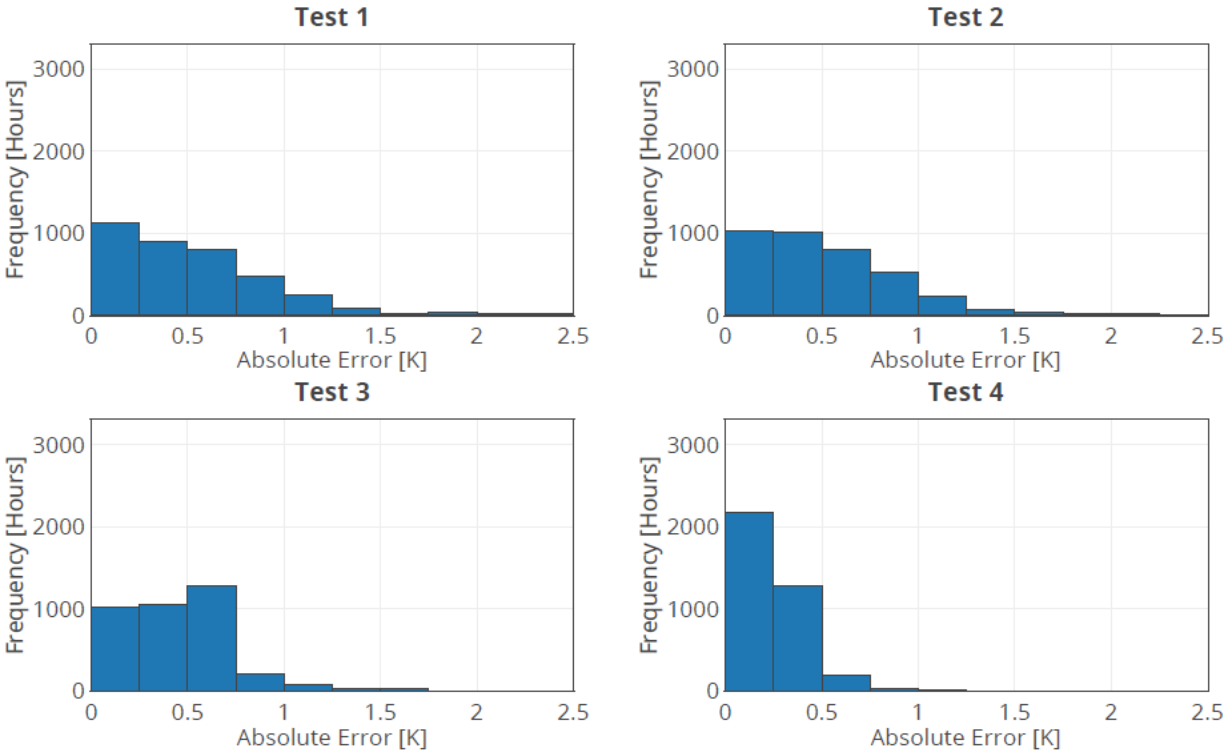

Figure 13. MAE Histograms for Tests 1-4 (Ensemble Calibration with variable glazing parameters)

4.5 Augmented Ensemble Calibration

Table 7 shows the metrics obtained via the application of Augmented Ensemble Calibration. Note that the calibration metrics of the baseline scenario (Test 1) has identical values to the ones reported in Table 4 since the Augmented Ensemble Calibration uses the Ensemble model calibrated in Section 4.2 as a model input. The other test cases are calibrated with an accuracy similar to the one described in Table 4. In fact, Tests 3 and 4 are better calibrated when glazing is used as a variable parameter through model augmentation. This phenomenon is similar to the one described in Section 4.2 (a larger number of insulated models will slightly bias the calibration). However, it is also worth noting that highly insulated models are less likely to be impacted by fluctuations in outdoor temperature and thus the models are calibrated to a higher level of accuracy.

Metric	*Test 1*	*Test 2*	*Test 3*	*Test 4*
MAE	0.262	0.232	0.127	0.121
$RMSE$	0.325	0.289	0.158	0.151
MBE	-0.030	-0.155	-0.069	-0.328

Table 7. Performance Metrics for Augmented Ensemble Calibration

Figures 14 and 15 shows that the dynamic response of the Augmented Ensemble Calibration framework, which features the infiltration model described in Section 3.4, is comparable with Ensemble Calibration prior to glazing retrofit and infiltration modelling (Figures 6 and 7). Furthermore, Figure 15 shows that the average error distributions are negatively skewed when compared with the distributions shown in Figure 13. This implies a more accurate model calibration. The performance of Test 1 remains the same as in Figures 6 and 7 because the Augmentation algorithm does not alter the baseline (i.e., pre-retrofit) model.

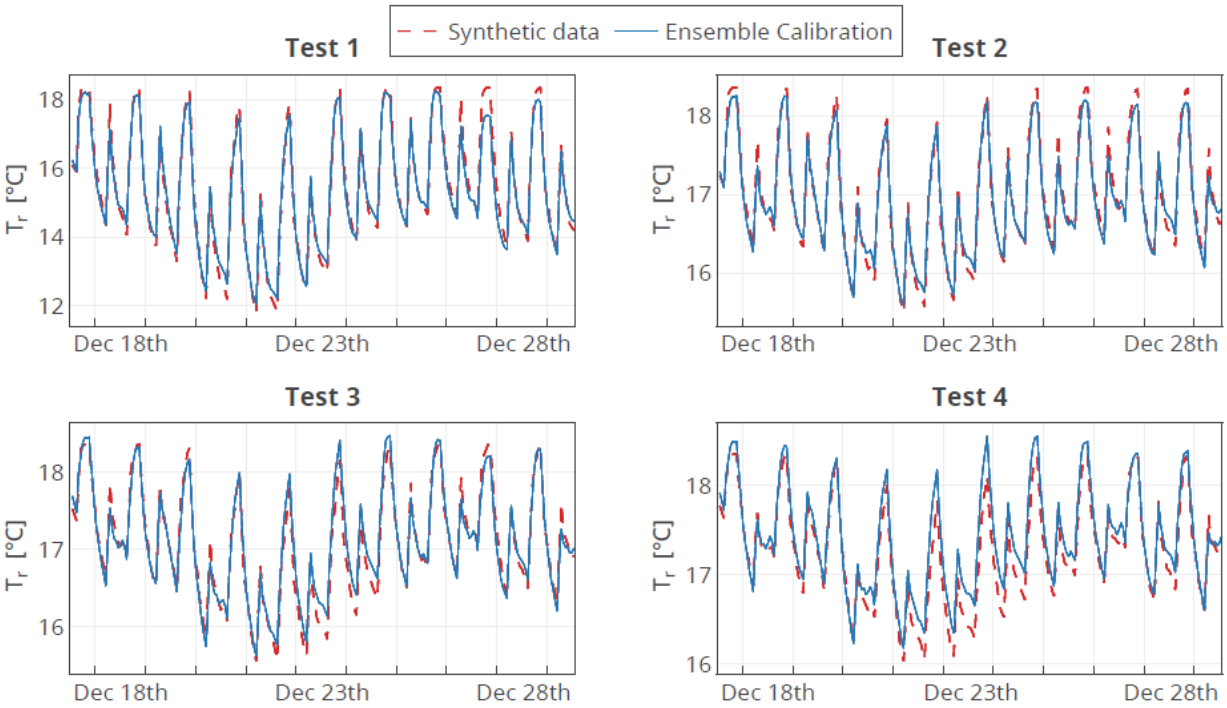

Figure 14. Model Response for Tests 1-4 (Augmented Ensemble Calibration)

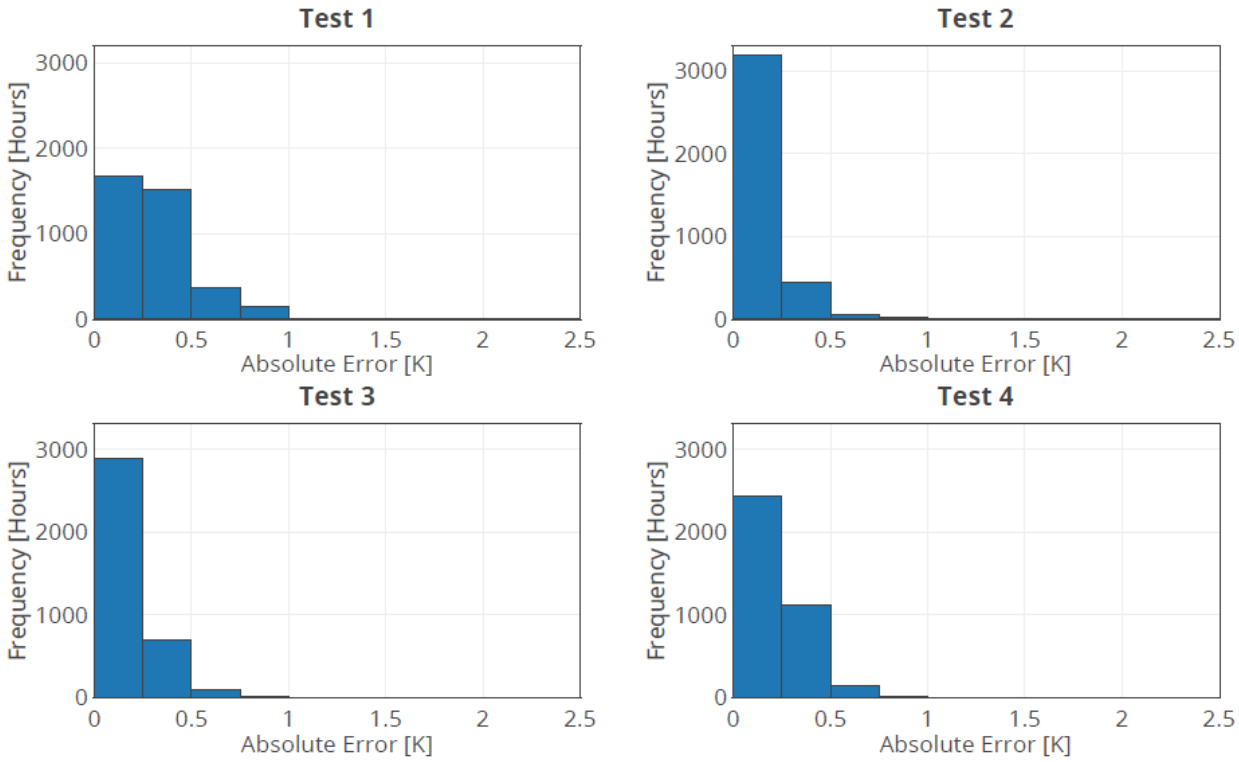

Figure 15. MAE Histograms for Tests 1-4 (Augmented Ensemble Calibration)

To conclude, Table 8 and Figure 16 summarize the performance of the proposed calibration algorithms after the infiltration model is incorporated. For simplicity purposes, the $RMSE$ is considered as a comparison metric. The proposed Augmented Ensemble Calibration methodology results in a comparable performance with respect to the Ensemble Calibration method for Tests 2-4. The models are not directly comparable because Augmented Ensemble Calibration features glazing information, whereas the Ensemble Calibration algorithm does not. In contrast, the Ensemble Calibration algorithm featuring glazing parameters as variable parameters results in a less accurate calibration for all Test cases, even for the best case scenario for this method (i.e., Calibration Run 3). Hence the relevance of the proposed methodology.

Algorithm	*Test 1*	*Test 2*	*Test 3*	*Test 4*
Ensemble Calibration	0.334	0.316	0.235	0.228
Ensemble Calibration (infiltration model)	0.325	0.320	0.214	0.205
Ensemble Calibration (variable glazing parameters)	0.622	0.641	0.506	0.316
Augmented Ensemble Calibration (glazing and infiltration)	0.325	0.289	0.158	0.151

Table 8. Calibration accuracy of the proposed algorithms (RMSE only)

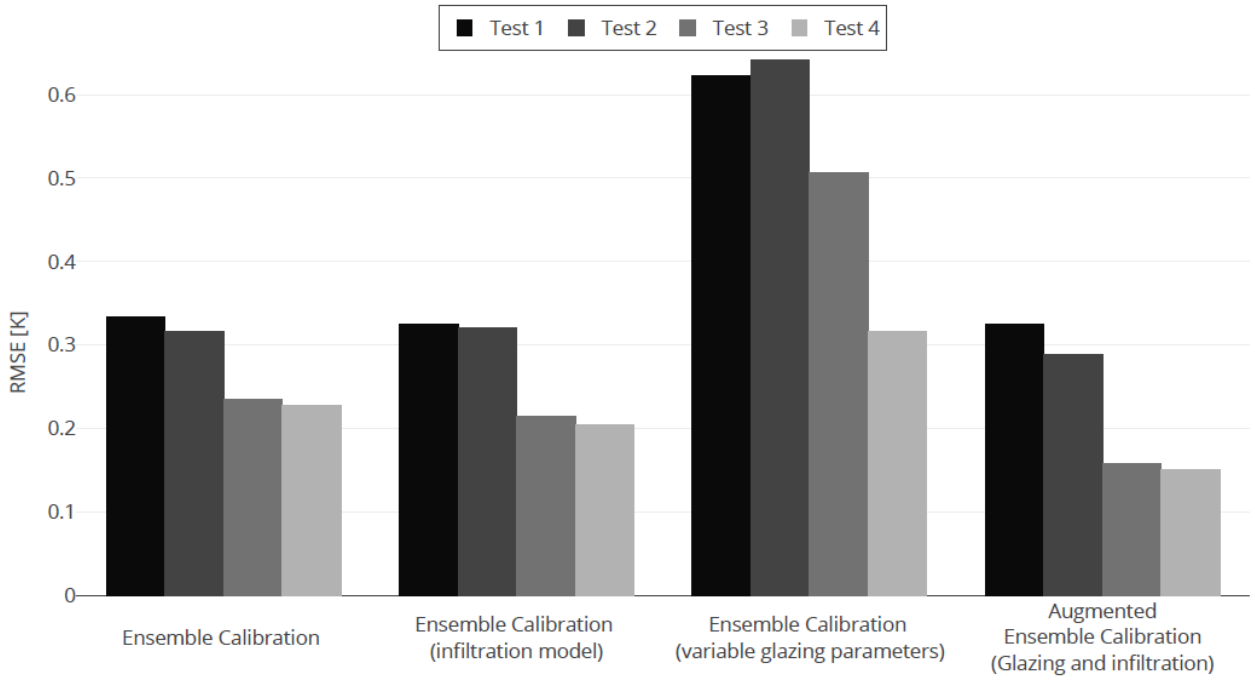

Figure 16. Computational Performance of the Calibration Algorithms

4.6 Computational performance of the Augmented Ensemble Calibration method

Figure 17 compares the numerical performance and the computational performance of the best performing Ensemble Calibration, Ensemble Calibration with glazing retrofits and Augmented Ensemble Calibration after four runs of each algorithm. The computations were carried out using a Dell Server PER 730 server with 2 Intel Xeon E5-2699 processors at a frequency of 2.20 GHz and 128 GB of memory. For computational evaluation purposes, only 8 cores were used at a single time. The Ensemble Calibration executes in slightly over an hour (79.16 minutes). The computational cost of the additional dimensions (i.e., u_{win} and g_{win} as a retrofit parameter) is 493.80 minutes (i.e., 6.2 times slower than Ensemble Calibration). The augmentation algorithm results in an average computational run of 12.64 minutes. However, this average time needs to be multiplied by a factor of 3 because the algorithm needs to be run for each glazing scenario beyond the baseline glazing parameters value. Hence, the total computational time of the Augmented Ensemble Calibration algorithm (including the time required to compute the original Ensemble) is 126.38 minutes. Thus, the Augmented Ensemble Calibration is a faster algorithm (i.e., 3.9 times faster) which is preferable to using an inaccurate higher dimensional Ensemble Calibration with glazing parameters as variable parameters.

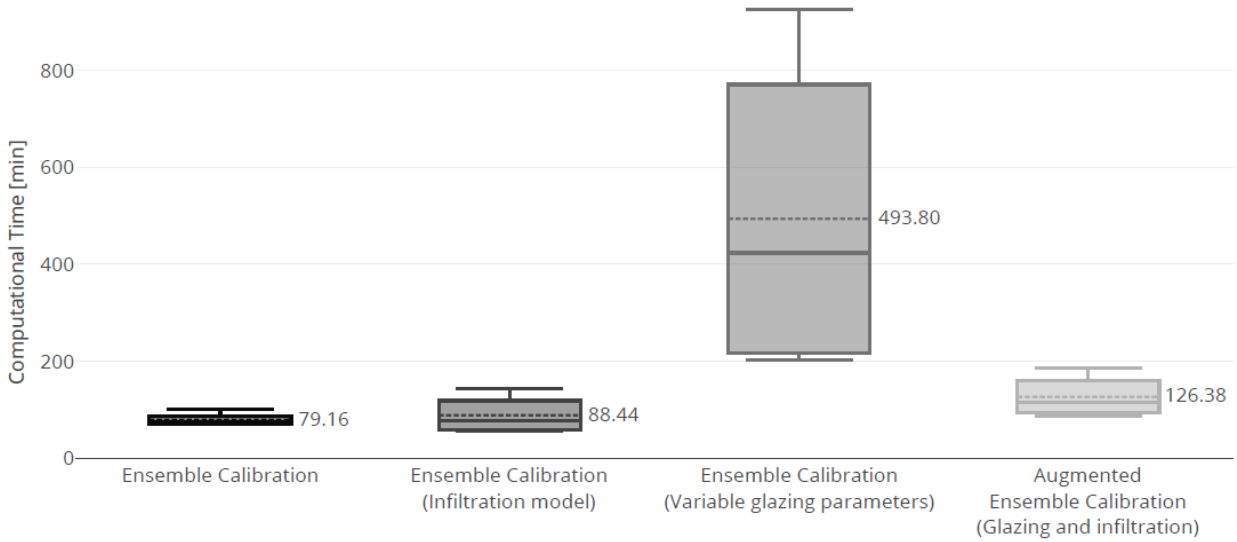

Figure 17. Computational performance of the calibration algorithms

5. Conclusions

The current study introduces an algorithm to augment the capabilities of Ensemble Calibration by means of adding the thermal effects of window retrofit and the estimated reduction of air tightness due to the addition of ECM measures. The current study demonstrated that glazing parameters cannot be added post Ensemble Calibration. It was also shown that incorporating glazing parameters as part of the Ensemble Calibration methodology results in an inaccurate calibration due to the sensitivity of the cost function (i.e., calibration error) with respect to highly sensitive parameters (e.g., glazing and infiltration parameters). The proposed approach exploits the knowledge of glazing and infiltration values (which can be readily extracted from the archetype) to incorporate glazing retrofits and infiltration reduction scenarios by adding augmentation functions to the original Ensemble model, thus minimizing the error in calibration that may result from merely adding the glazing information post Ensemble Calibration. Furthermore, this discrete-event modelling suits the incorporation of the simplified infiltration reduction model with relative ease.

Ensemble Calibration uses a computationally intensive algorithm. The use of PSO (or other heuristics) as a core optimisation engine requires the solution of a large number of function evaluations to obtain an accurately calibrated Ensemble. Furthermore, the method is sensitive to the initial PSO seed and there is no guarantee that a single run of the Ensemble Calibration model will yield an accurate calibration. In practice, four runs of the algorithm are deemed sufficient for the acquisition of an accurate Ensemble model.

The Ensemble Calibration framework (and thus the Augmented Ensemble Calibration) results in a reduced penalty in the performance of the baseline model to the detriment of the calibration of the other elements of the Ensemble. Alleviating such penalty would require the study of composite cost functions which would weigh the performance of the baseline model against the other models

The current paper expands the Ensemble Calibration methodology by means of featuring glazing and infiltration retrofit decision making. All models are still related to the pre-retrofitted model and therefore the models are still linearly dependent. Therefore, a linearization heuristic can find the optimal retrofit configuration and power systems configuration (e.g., optimal electricity load dispatch for different ECM configurations). Future work will focus on the implementation of the augmented Ensemble models for the integrated analysis of retrofit policies at a national scale using a linearization heuristic. Additional work is required to expand the geometry of the models calibrated using Ensemble Calibration via model aggregation.

Acknowledgements

This project has received funding from the European Union's Horizon 2020 research and innovation programme under grant agreement No 646116.

William Turner is supported by the Science Foundation Ireland Strategic Partnership Programme (SFI/15/SPP/E3125) and the UCD Energy21 program, co-financed through the Marie Sklodowska-Curie program (FP7-PEOPLE-2013-COFUND).

References

AECOM. 2013. “Cost Optimal Calculations and Gap Analysis for Recast EPBD for Residential Buildings,” no. March 2013: 48,79,95.

Alley, R B, B Hewitson, B J Hoskins, F Joos, J Jouzel, V Kattsov, U Lohmann, et al. 2016. *Climate Action Now - Summary for Policymakers*.

Andrade-Cabrera, Carlos, Daniel Burke, William J N Turner and Donal P Finn. 2017. “Ensemble Calibration of Lumped Parameter Retrofit Models Using Particle Swarm Optimization.” *Energy & Buildings* 155. Elsevier B.V.: 513–32.

Andrade-Cabrera, Carlos, William J.N. Turner, Daniel Burke, Olivier Neu and Donal P Finn. 2016. “Lumped Parameter Building Model Calibration Using Particle Swarm Optimization.” In *3rd Asia Conference of International Building Performance Simulation Association (ASIM 2016)*.

ASHRAE. 2012. “International Weather for Energy Calculations 2.0 (IWEC Weather Files).” Atlanta, GA: ASHRAE.

ASHRAE. 2017. *2017 ASHRAE Handbook—Fundamentals*. ASHRAE. Atlanta, GA.

Ault, Graham, Joe Clarke, Simon Gill, Jon Hand, Jaemin Kim, Ivana Kockar and Katalin Svehla. 2013. “The Use of Simulation to Optimise Scheduling of Domestic Electric Storage Heating within Smart Grids.” In *Proc. 2nd IBPSA - England Conference (BSO2014)*. Chambery, France.

Bakirtzis, Grigorios A., Pandelis N. Biskas and Vasilis Chatziathanasiou. 2012. “Generation Expansion Planning by MILP Considering Mid-Term Scheduling Decisions.” *Electric Power Systems Research* 86. Elsevier B.V.: 98–112.

Cerezo, Carlos, Julia Sokol, Saud AlKhaled, Christoph Reinhart, Adil Al-Mumin and Ali Hajiah. 2017. “Comparison of Four Building Archetype Characterization Methods in Urban Building Energy Modeling (UBEM): A Residential Case Study in Kuwait City.” *Energy and Buildings* 154. Elsevier B.V.: 321–34.

Crabb, J. A., N. Murdoch and J.M. M. Penman. 1987. “A Simplified Thermal Response Model.” *Building Services Engineering Research and Technology* 8 (1): 13–19.

Dickerhoff, D.J., D.T. Grimsrud and R.D. Lipschutz. 1982. “Component Leakage Testing in Residential Buildings.” *Summer Study in Energy Efficient Buildings*, no. February.

EEA. 2015. “The European Environment: State and Outlook: 2015 - Executive Summary.”

European Climate Foundation. 2010. “Roadmap 2050：A Practical Guide to a Prosperous, Low-Carbon Europe,” no. April: 99.

European Climate Foundation ECF. 2011. “Power Perspectives 2030: On the Road to a Decarbonised Power Sector.” *Full Report*, 1–85.

Fumo, Nelson. 2014. “A Review on the Basics of Building Energy Estimation.” *Renewable and Sustainable Energy Reviews* 31. Elsevier: 53–60.

Gillott, M. C., D. L. Loveday, J. White, C. J. Wood, K. Chmutina and K. Vadodaria. 2016. “Improving the Airtightness in an Existing UK Dwelling: The Challenges, the Measures and Their Effectiveness.” *Building and Environment* 95. Elsevier Ltd: 227–39.

Greensfelder, Erik M., Gregor P. Henze and Clemens Felsmann. 2011. “An Investigation of Optimal Control of Passive Building Thermal Storage with Real Time Pricing.” *Journal of Building Performance Simulation* 4 (2): 91–104.

Hassan, Rania and Babak Cohanim. 2005. “A Comparison of Particle Swarm Optimization and the Genetic Algorithm.” *1st AIAA Multidisciplinary Design Optimization Specialist Conference*, 1–13.

He, Xiaofei, Zijun Zhang and Andrew Kusiak. 2014. “Performance Optimization of HVAC Systems with Computational Intelligence Algorithms.” *Energy and Buildings* 81. Elsevier B.V.: 371–80.

Hong, Sung, Tadj Oreszczyna and Ridley Ian. 2004. “The Impact of Energy Efficient Refurbishment on the Airtightness in English Dwellings.” In *25th AIVC (Air Infiltration and Ventilation Centre) Conference*.

IPCC. 2014. “Climate Change 2014 Synthesis Report Summary Chapter for Policymakers.” *Ipcc*, 31.

Jermyn, Denver and Russell Richman. 2016. “A Process for Developing Deep Energy Retrofit Strategies for Single-Family Housing Typologies: Three Toronto Case Studies.” *Energy and Buildings* 116. Elsevier B.V.: 522–34.

Kinnane, Oliver, Derek Sinnott and William J N Turner. 2016. “Evaluation of Passive Ventilation Provision in Domestic Housing Retrofit.” *Building and Environment* 106. Elsevier Ltd: 205–18.

Kusiak, Andrew and Guanglin Xu. 2012. “Modeling and Optimization of HVAC Systems Using a Dynamic Neural Network.” *Energy* 42 (1). Elsevier Ltd: 241–50.

Lorenz, F. and G. Masy. 1982. “Methode D’evaluation de L’economie D’energie Apporte Par L’intermittence de Chauffage Dans Les Batiments. Traitement Par Differences Finies D’un Model a Deux Constantes de Temps.” Liege, Belgium.

Marino, Simeone, Ian B. Hogue, Christian J. Ray and Denise E. Kirschner. 2008. “A Methodology for Performing Global Uncertainty and Sensitivity Analysis in Systems Biology.” *Journal of Theoretical Biology* 254 (1): 178–96.

Mathworks. 2015. “Global Optimization Toolbox - User’s Guide.”

Muringathuparambil, Reshmi Joseph, Josephine Kaviti Musango, Alan C. Brent and Paul Currie. 2017. “Developing Building Typologies to Examine Energy Efficiency in Representative Low Cost Buildings in Cape Town Townships.” *Sustainable Cities and Society* 33 (May). Elsevier: 1–17.

Neu, Olivier, Simeon Oxizidis, Damian Flynn, Fabiano Pallonetto and Donal Finn. 2013. “High Resolution Space - Time Data: Methodology for Residential Building Simulation Modelling.” *13th Conference of International Building Performance Simulation Association*, 2428–35.

Pudjianto, Danny, Marko Aunedi, Predrag Djapic and Goran Strbac. 2014. “Whole-Systems Assessment of the Value of Energy Storage in Low-Carbon Electricity Systems.” *IEEE Transactions on Smart Grid* 5 (2). IEEE: 1098–1109.

Reinhart, Christoph F and Carlos Cerezo Davila. 2016. “Urban Building Energy Modeling – A Review of a Nascent Field.” *Building and Environment* 97. The Authors: 196–202.

Robertson, A F and Daniel Gross. 1958. “An Electrical-Analog Method for Transient Heat-Flow Analysis.” *Journal of Research of the National Bureau of Standards* 61 (2): 105–15.

Sinnott, Derek. 2016. “Dwelling Airtightness: A Socio-Technical Evaluation in an Irish Context.” *Building and Environment* 95. Elsevier Ltd: 264–71.

Sokol, Julia, Carlos Cerezo Davila and Christoph F. Reinhart. 2017. “Validation of a Bayesian-Based Method for

Defining Residential Archetypes in Urban Building Energy Models." *Energy and Buildings* 134. Elsevier B.V.: 11–24.

Wu, Raphael, Georgios Mavromatidis, Kristina Orehounig and Jan Carmeliet. 2017. "Multiobjective Optimisation of Energy Systems and Building Envelope Retrofit in a Residential Community." *Applied Energy* 190. Elsevier Ltd: 634–49.

Appendix A: Augmented Ensemble Calibration Algorithm

Algorithm 1: Augmented Ensemble Calibration

Result: Parametric evolution for glazing scenarios V_P: $\{\bar{R}^{\star}_{ext_2 N,M,O,P}, \bar{R}^{\star}_{ext_3 N,M,O,P}, \bar{R}^{\star}_{ceil_1 N,M,O,P}\}$

Pre-Computed: Synthetic time series $T_{r,data}$, $T_{attic,data}$, u_{data} and d_{data}

Baseline model parameters p_0, including fixed parameters F and baseline fixed parameters $R^{\star}_{ext_2,0}$, $R^{\star}_{ext_3,0}$ and $R^{\star}_{ceil_3 c}$

Ensemble function parameters prior to augmentation $\alpha_{ext,M,O}$, $\beta_{ext,M,O}$, $\alpha_{int,N,O}$, $\beta_{int,N,O}$, $\alpha_{ceil,N,M}$ and $\beta_{ceil,N,M}$

Pre-defined variable parameters $V_P = \{\bar{R}_{ext_2 N,M,O,P}, \bar{R}_{ext_3 N,M,O,P}, \bar{R}_{ceil_1 N,M,O,P}\}$

Known: Building geometry information

Assumptions: Baseline glazing and infiltration properties: $u_{win,0}$, $g_{win,0}$ and ACH_0

1 Define upper and lower boundaries for the growth parameters $\mu_{ext,M,O,P}$, $\nu_{ext,M,O,P}$, $\mu_{int,N,O,P}$, $\nu_{int,N,O,P}$, $\mu_{ceil,N,M,P}$ and $\nu_{ceil,N,M,P}$

2 Call the PSO routine with particles $p(i) = \{V_P(i)\}$

3 **while** $Convergence = False$ **do**

4 Initialize the global cost $J_{global}(p(i)) = 0$

5 **for** $M = 1{:}\, n_{ext}$

6 **for** $N = 1{:}\, n_{int}$

7 **for** $O = 1{:}\, n_{ceil}$

8 **for** $P = 1{:}\, n_{win}$

9 Update model parameters V_P (Algorithm 2)

10 Calculate the continuous-time building model with p_0, $V_{N,M,O}$ and $V_{P\,N,M,O,P}$

11 Discretize the model and evaluate the local solution cost $\mathrm{J}_{\mathrm{local}}(p_0, V_{N,M,O}, V_{P\,N,M,O,P})$ (Equation 2)

12 Update the global solution cost $\mathrm{J}_{\mathrm{global}}(p(i)) = \mathrm{J}_{\mathrm{global}}(p(i)) + \mathrm{J}_{\mathrm{local}}(p_0, V_{N,M,O}, V_{P\,N,M,O,P})$

13 **End**

14 **End**

15 **End**

16 **End**

17 Update $p(i)$ until convergence of the PSO solver (Mathworks 2015)

28 **end**

Algorithm 2: Model Update Subroutine

Result: Parametric evolution for glazing scenarios V_P: $\{\bar{R}^{\star}_{ext_2 N,M,O,P}, \bar{R}^{\star}_{ext_3 N,M,O,P}, \bar{R}^{\star}_{ceil_1 N,M,O,P}\}$

Update the infiltration assumption $\overline{ACH}_{inf}$ with the appropriate fraction f_{inf} (Equation 5)

Update the glazing parameters $u_{win} = \bar{u}_{win}(P)$ and $g_{win} = \bar{g}_{win}(P)$

if $M > 1$ then

    Calculate wall resistance ($\bar{R}_{ext_2 N,M,O,P}$) with parameters $\mu_{ext,N,O,P}$ and $\nu_{ext,N,O,P}$ (Equation 6)

End

if $N > 1$ then

    Calculate wall resistance ($\bar{R}_{ext_2 N,M,O,P}$) with parameters $\mu_{int,M,O,P}$ and $\nu_{int,M,O,P}$ (Equation 6)

End

if $O > 1$ then

    Calculate wall resistance ($\bar{R}_{ceil_2 N,M,O,P}$) with parameters $\mu_{ceil,N,M,P}$ and $\nu_{ceil,N,M,P}$ (Equation 6)

end